Trends in Analytical Chemistry 166 (2023) 117172

Contents lists available at ScienceDirect

Trends in Analytical Chemistry

journal homepage: www.elsevier.com/locate/trac

High-throughput single-cell analysis of nanoparticle-cell interactions

Majood Haddad [a, 1], Alex N. Frickenstein [a, 1], Stefan Wilhelm [a, b, c, *]

[a] Stephenson School of Biomedical Engineering, University of Oklahoma, Norman, OK, 73019, USA
[b] Stephenson Cancer Center, University of Oklahoma Health Sciences Center, Oklahoma City, OK, 73104, USA
[c] Institute for Biomedical Engineering, Science, and Technology (IBEST), University of Oklahoma, Norman, OK, 73019, USA

ARTICLE INFO

Article history:
Received 7 March 2023
Received in revised form
1 July 2023
Accepted 2 July 2023
Available online 10 July 2023

Keywords:
Single-cell analysis
Single-nanoparticle analysis
Flow cytometry
Inductively coupled plasma mass spectrometry
Mass cytometry
Nano-bio interactions

ABSTRACT

Understanding nanoparticle-cell interactions at single-nanoparticle and single-cell resolutions is crucial to improving the design of next-generation nanoparticles for safer, more effective, and more efficient applications in nanomedicine. This review focuses on recent advances in the continuous high-throughput analysis of nanoparticle-cell interactions at the single-cell level. We highlight and discuss the current trends in continual flow high-throughput methods for analyzing single cells, such as advanced flow cytometry techniques and inductively coupled plasma mass spectrometry methods, as well as their intersection in the form of mass cytometry. This review further discusses the challenges and opportunities with current single-cell analysis approaches and provides proposed directions for innovation in the high-throughput analysis of nanoparticle-cell interactions.

1. Introduction

Creating safe, effective, and efficient nanomedicines for biomedical applications requires a thorough understanding of how administered nanoparticles interact with cells [1,2]. These so-called nanotechnology-biology "nano-bio" interactions are complex and can occur with a broad range of efficiency, selectivity, and specificity, which is partially attributed to the substantial cell heterogeneity in both healthy and diseased tissues [3]. Nanoparticles used in nanomedicine are often defined as 1–100 nm particles and can be comprised of inorganic or organic materials [4]. Their targeted clinical application vary from therapeutic drug delivery, imaging diagnostics, and vaccination [5–8]. At the core of each of these applications are nano-bio interactions that dictate nanoparticle fate, safety, and efficacy. To better probe and understand the interactions between nanoparticles and cells, researchers require robust analytical techniques to spatiotemporally resolve these nano-bio interactions at the single-cell and single-nanoparticle levels. This research has the potential to guide the engineering of safer and more effective nanomedicines for improved clinical outcomes [9,10].

Single-cell analysis allows for increased resolution and understanding of cellular mechanisms and behaviors relative to nano-bio interactions. It is well understood that nanoparticle characteristics such as size, shape, and surface chemistry influence nano-bio interactions [11–18]. Detailed understanding of how nanoparticle characteristics influence nano-bio interactions is required to improve nanomedicine clinical safety and efficacy.

While batch mode, population-based analysis can provide insight into broad trends in nano-bio interactions based on changes in nanoparticle characteristics, batch analysis fails to indicate the cellular or subcellular distribution of nanoparticles in cells. Additionally, batch analysis relies upon assumptions that may not hold true for all samples, such as the assumption that all cells contain nanoparticles or that all nanoparticles have the same size, shape, and mass.

Single-cell analysis allows for distribution analysis to understand the range of nano-bio interactions for a given system and can identify cells that contain no nanoparticles after treatment. Additionally, for blood or tissue samples comprised of a complex cellular milieu, single-cell analysis allows for the identification and quantification of different cell identities (i.e., phenotypes) and corresponding nano-bio interactions on a per-cell basis that can point

* Corresponding author. Stephenson School of Biomedical Engineering, University of Oklahoma, Norman, OK, 73019, USA.
E-mail address: stefan.wilhelm@ou.edu (S. Wilhelm).
[1] These authors contributed equally to this work.

https://doi.org/10.1016/j.trac.2023.117172
0165-9936/

Abbreviations

FCM	Flow Cytometry
FSC	Forward Scattering
ICP-MS	Inductively Coupled Plasma Mass Spectrometry
LA-ICP-MS	Laser Ablation ICP-MS
CyTOF	Mass Cytometry
nFCM	Nano-Flow Cytometry
PMT	Photomultiplier
PAFC	Photoacoustic Flow Cytometry
PAIFC	Photoacoustic Imaging Flow Cytometry
ICP-Q-MS	Quadrupole ICP-MS
SSC	Side Scattering
TOF-ICP-MS	Time-of-Flight ICP-MS

towards valuable nanoparticle design strategies. For example, by identifying how nanoparticles may have increased or decreased interactions with particular cell types in complex cellular systems (e.g., tissues), nanomedicines may be better engineered for enhanced safety and efficacy, Further, where possible, imaging of cells during single-cell analysis increases data value and provides opportunity for correlating nanoparticle quantity with sub-cellular accumulation.

Current methods of analyzing nano-bio interactions at the cellular level include, amongst others, microscopy [19–21], flow cytometry [22,23], and mass spectrometry [24,25]. Each of these approaches allows for the visualization, analysis, and/or quantification of cells at varying degrees of spatial and temporal resolution. Importantly, both flow cytometry and mass spectrometry allow for a continual flow analysis of cell samples. Such continual flow analysis is advantageous for the high-throughput quantification of cell phenotypes and associated nano-bio interactions at the single-cell level.

In this review, we highlight current technologies and advancing trends in continual flow, high-throughput analysis used to assess nanoparticle-cell interactions with single-cell resolution and, as possible, single-nanoparticle resolution. We focus our overview on flow cytometry and mass spectrometry approaches, as well as the intersection of these two methods in the form of mass cytometry. The advantages and considerations of each technique are discussed while highlighting areas of current investigation and future growth to advance the study of nano-bio interactions at the single-cell level.

2. Flow cytometry

Multiple approaches for flow cytometry have been employed to assess nano-bio interactions at the single-cell level. Table 1 provides a summary of selected recent studies in this research area. We discuss four different methods from the recently published literature, including conventional flow cytometry, imaging flow cytometry, photoacoustic (imaging) flow cytometry, and *in vivo* flow cytometry, and how these analytical methods have been used to study nano-bio interactions.

2.1. Conventional flow cytometry

Conventional flow cytometry is a technique in which individual cells are passed through a microfluidic system and subsequently illuminated by a laser source [23,62]. Upon interaction of the cells with the laser light, the scattered light and any fluorescence emissions are detected and quantified. This analysis provides insight into various cell parameters, including cell identity, phenotype, and viability. Light scattered from an individual cell is typically quantified in a label-free way as side scattering or forward scattering depending on whether the scattered light is detected orthogonally to the laser or in the same axis as the laser, respectively [63]. Generally, the label-free side scattering signal correlates with cell granularity or complexity, while the label-free forward scattering signal correlates with cell size. Besides light scattering, the laser may also excite fluorescence emissions from dyes used to label the cells, thus allowing for the identification and quantification of cells based on the specific fluorescence emission profiles [64].

Upon interaction with cells, nanoparticles can contribute to the label-free side scattering and forward scattering signals detected by the flow cytometer (Fig. 1A) [29,65]. The nanoparticle contribution to side scattering signal varies based on both the nanoparticle type and nanoparticle concentration. The effect of nanoparticle concentration on the side scattering signal was reported in a study by Youhannavee et al. An increase in magnetite nanoparticle concentration resulted in an increase in detected side scattering signal due to increased nanoparticle-cell interactions (Fig. 1B) [36]. This same study further showed how nanoparticle uptake varies by cell type. For the same magnetite nanoparticle concentration, PC3 human epithelial cancer cells showed increased nanoparticle-cell interactions compared to BPH1 human healthy epithelial cells. Other studies have reported similar trends whereby after increasing the nanoparticle concentration, cells more readily interact with nanoparticles, which results generally in an increase in label-free flow cytometry side scattering signal [26,30].

Additionally, the forward scattering signal can be used to check for apoptotic cells. FSC changes when cells die due to apoptosis. Cells that undergo apoptosis have a decreased forward scattering signal as the cell size decreases due to cell shrinkage, while the side scattering signal increases due to changes in cell granularity associated with the formation of apoptotic bodies within the cell [66]. Tracking these changes in cell scattering signal can be used to determine the effect of nanoparticle concentration or toxicity on cells. For instance, Taccola et al. found that the threshold value at which ZnO nanoparticles start inducing cell death in SH-SY5H human neuroblastoma cells is at a concentration of 0.42 mM. The authors used propidium iodide stain to compare live versus dead cells and confirm that the decrease in measured forward scattering signal is due to the threshold concentration value of the nanoparticles [67].

Conventional flow cytometry is further capable of detecting how differences in nanoparticle surface chemistry affect cellular interactions [34]. In a study by Zucker et al., silver nanoparticles (AgNPs) of varying surface modifications, i.e., branched poly (ethyleneimine) (bPEI), citrate (CIT) polyvinylpyrrolidone (PVP), and poly (ethylene glycol) (PEG), were used to treat ARPE-19 human epithelial cells. Significant differences in the measured side scattering signals were observed between the different AgNP surface chemistries when cells were assessed with label-free flow cytometry after nanoparticle incubation [28]. Cells treated with positively charged AgNP-bPEI demonstrated greater side scattering signals by 3–6 fold compared to the other tested surface chemistries. A similar experiment by Chakraborty et al. was performed using gold nanorods (GNRs). The nanoparticles were surface-modified with PEG, poly (allylamine hydrochloride) (PAH), polystyrene sulfonate (PSS), or CIT the corresponding nanoparticle-cell interactions with human THP1 differentiated M1 and M2 macrophages were assessed by label-free flow cytometry. The greatest side scattering signal in both M1 and M2 macrophages was measured in cells treated with positively charged PAH-GNRs [68]. These observations are in line with reports by Lee et al. and Donahue et al., who used

Table 1
Selected nano-bio interaction studies using different flow cytometry approaches.

Approach	Nanoparticle Type	Nanoparticle Size (nm)	Nanoparticle Function	Cell Line(s)	Notable Methods	Ref.
Conventional Flow Cytometry/ FACS[a]	Silver	10, 50, and 100 nm	Affects expression of Toll-like receptors	RAW264.7 mouse leukemia cells	Allows for sorting of cells	[26]
	Silver	10, 50, and 75 nm	Affects cell growth and nanoparticle uptake	ARPE-19 human epithelial cells	Analysis of nanoparticle cell uptake based on the combination of light scattering and far-red fluorescence	[27]
	Silver	80 nm	Affects nanoparticle uptake	ARPE-19 human epithelial cells	Analysis of how different nanoparticle surface modifications affect nanoparticle cell uptake	[28]
	Gold nanospheres, Gold nanorods	26 nm and 67 nm × 33 nm, respectively	Used as intracellular imaging probes or as therapeutic reagents	MDA-MB-231 human breast cancer cells	Use of more red-shifted excitation lasers to enhance the optical signal of flow cytometry	[29]
	Gold	40, 60, 80, and 100 nm	Internalization in many different types of cells	HeLa human cervical cancer cells	Label-free quantification of nanoparticles within cells	[30]
	TiO_2	<10 nm	Chemical inertness	NIH/3T3 mouse fibroblasts and A549 human pulmonary cancer cells	Analysis of nanoparticle-cell interactions via fluorescence	[31]
	ZnO and TiO_2	30 and 50 nm, respectively	Commercially relevant in consumer products and nanodevices	*Escherichia coli* bacterial cells	Detection of nanoparticle uptake in bacteria	[32]
	TiO_2, SiO_2, CeO_2, and ZnO	TiO_2: ~168 nm −1um; SiO_2: 175−250 nm; CeO_2: <10 nm and <25 nm; ZnO: ~41.5 nm	Understanding of nanoparticle ecotoxicological effects	Freshwater algae (Raphidocelis subcapitata, Desmodesmus subspicatus, and Chlorella vulgaris)	Analysis of nanoparticle uptake in microalgae	[33]
	Ultrasmall nanoparticles	2 nm	Understanding protein corona interactions	A549 human pulmonary cancer cells	Detection of nanoparticle (<5 nm in diameter) interactions with cells	[34]
	CuS	8 nm	Evaluation of biocompatibility and toxicity	HeLa human cervical cancer cells	Photothermal efficiency analysis of the nanoparticles to determine cell viability	[35]
	Magnetite nanoparticles	10 nm	Relevant nanomaterial for diagnosis and cancer therapy	PC3 human cancer epithelial cells and BPH1 human healthy epithelial cells	Label-free quantification of various concentrations of nanoparticles with different surface chemistries within cells	[36]
	$NaYbF_4$@$NaYF_4$	~18 nm	Used due to their high stability, large anti-Stokes shift, and narrow emission bandwidth	A549 human pulmonary cancer cells	Examines side scattering vs. fluorescence intensity of the single-cell suspension rather than comparing side scattering to forward scattering	[37]
	SiO_2	~27 nm and ~70 nm	Enhanced (colloidal) stability	A549 human pulmonary cancer cells	Analysis of fluorescence intensity of nanoparticles rather than side scattering of the single-cell suspension	[38]
	Fluorescently-labeled polystyrene nanoparticles	40, 100, and 200 nm	Nanoparticle size tunability	HeLa human cervical cancer cells	Detection of nanoparticle interactions with various intracellular organelles	[39]
	Fluorescently-labeled polystyrene nanoparticles	100 nm	Size tunability	MDA-MB-231 human breast cancer cells	Correlation of nanoparticle uptake with cell size rather than cell complexity	[40]
	Fn14-Targeted polymeric nanoparticles	~96−163 nm	Used due to their prolonged systemic circulation, enhanced tumor accumulation, and extended tissue penetration and drug release	Human MDA-MD-231-TD-luciferase triple negative breast cancer cells	Uptake analysis of fluorescently labeled nanoparticles by cells	[41]
	Polymeric nanoparticles	~45 nm	Used due to their ability to label cells, and usage in imaging modalities	Primary macrophages	Analysis of nanoparticle-labeled cells	[42]
	Polymeric nanoparticles	128 nm	Used due to their abilities to scavenge reactive oxygens, serving as an effective therapy for atherosclerosis	RAW264.7 mouse leukemia cells	Analysis of fluorescence intensity of nanoparticles rather than side scattering of the single-cell suspension	[43]
	Gag-based virus-like particles	161 and 184 nm	Used due to their potential as candidates for recombinant vaccine development	Insect-derived cells (S. frugiperda and T. ni BTI-TN-5B1-4)	Allows for baculovirus infection process comparison between different insect cell lines	[44]
Imaging Flow Cytometry	SiO_2	50 nm	Used due to their ability to be easily labeled with different fluorochromes	NCI−H292 human pulmonary cancer cells	Evaluation of nanoparticle internalization at different temperatures	[45]
	Polymeric nanoparticles	~50 nm	Used due to their ability to enhance light absorption, induce	B16−F10 mouse melanoma skin cancer cells	Analysis of nano-bio interactions on an on-chip photoacoustic imaging flow cytometer	[46]

(*continued on next page*)

Table 1 (*continued*)

Approach	Nanoparticle Type	Nanoparticle Size (nm)	Nanoparticle Function	Cell Line(s)	Notable Methods	Ref.
			photoacoustic signals, and high cell viability			
	CD63-eGFP −transfected HEK293T extracellular vesicles	~104 nm	Used due to their inherent rapid proliferation, high EV yield, and ease of genetic manipulation	HEK293T human embryonic kidney cells	Imaging of sEVs down to 100 nm in diameter	[47]
	eGFP-labeled small extracellular vesicles	130 nm	Used due to their abundance, ability to control various processes and mediate complex intercellular interactions in a targeted manner	THP-1 human leukemia cells	Discrimination between single and coincidental sEVs	[48]
Photoacoustic (Imaging) Flow Cytometry	CuS	8.6 nm	Used due to their ability to specifically target ovarian circulating tumor cells and capability to emit a photoacoustic signal	SKOV-3 human ovarian cancer cells	Real-time imaging of sample	[49]
	CuS NPs	8.6 nm	Used due to their ability to enable specific binding of ovarian-cancer cells and PA detection	SKOV-3 human ovarian cancer cells	Detection of early-stage cancer metastasis	[50]
	Gold nanorods	25 × 113 nm	Used due to their ability to enable PA detection at the single-cell level	MDA-MB-231 human breast cancer cells and ZR-75-1 human breast cancer cells	Analysis of nanoparticle toxicity	[51]
	Streptavidin coated red fluorescent latex nanoparticles	320 nm	Used due to their ability to be detected and attached to breast cancer cells	T-47D human breast cancer cells	Detection of colocalized nanoparticles within breast cancer cells in a coculture sample	[52]
	Polymeric nanoparticles	Not Reported	Used to their ability to label cells, identify, and eliminate glioma cells	9 L mouse glioma cells, HeLa human cervical cancer cells, and C6 mouse glioma cells	Multiparametric labeling and identification of cells in a single workflow	[53]
In vivo Flow Cytometry	Pristine graphene flakes	1−1.2 nm	Used due to their tremendous potential in various medical applications	Red Blood Cells	Imaging of circulating GBN clusters in blood vessels and assessment of their kinetics	[54]
	Quantum dot-carbon nanotube conjugates	~5 nm	Used due to their ability to be photothermal, photothermal and fluorescent contrast agents	Plant xylem and phloem vascular systems	In vivo real-time photoacoustic monitoring of nanoparticle uptake in plants	[55]
	Gold nanorods	~10 × 35 nm	Used due to their ability to be used as magnetic−photothermal switchable probes	Melanoma cells	Uses high-pulse-repetition rate laser	[56]
	Gold nanorods	15 × 50 nm	Used due to their ability to label circulating cell tumors, allowing for the cells' detection	HTB-65 human melanoma cells, MALME-3M human melanoma skin cancer cells, and B16−F10 mouse melanoma skin cancer cells	Blood cancer testing using a high-pulse-repetition-rate diode laser	[57]
	Magnetic nanoparticles and golden carbon nanotubes	30 nm	Used due to their ability to target a breast cancer cells' receptor, and to improve detection sensitivity and specificity, respectively	MDA-MB-231 human breast cancer cells	Detection of cells in the bloodstream	[58]
	Polylactic acid	100 nm	Used due to their ability to circulate longer in the bloodstream and form less aggregates	Primary mouse monocytes	Simultaneous monitoring of monocytes and nanoparticles *in vivo*	[59]
	Polymeric nanoparticles	~107−122 nm	Used due to their effect to target and neutralize circulating tumor cells	4T1 mouse breast cancer epithelial cells	Detection of labeled cancer cells *in vivo* using polymeric modified and labeled nanoparticles	[60]
	Carbon nanotubes	Length: 186 nm; Diameter: 1.7 nm for the single-walled Length: 376 nm; Diameter: 19.0 nm for the multiwalled	Used due to their ability to be used as near infra-red high-photoacoustic contrast agent	*Escherichia coli* bacterial cells	Detection of labeled bacteria *in vivo*	[61]

[a] FACS = fluorescence-activated cell sorting.

inductively coupled plasma mass spectrometry to quantify the effect of positive surface charges on nanoparticle-cell interactions [25,69].

Conventional flow cytometry has also been used to assess how nanoparticle composition influences nano-bio interactions, as shown by Kumar et al. The researchers reported higher side scattering signals from *E. coli* bacterial cells exposed to TiO_2 nanoparticles compared to the same concentration of ZnO nanoparticles. The observed increase in the side scattering signal can be attributed to a greater degree of interaction between *E. Coli* and TiO_2 nanoparticles [32]. The authors attribute that signal increase to the size of the TiO_2 nanoparticles, in which the TiO_2 nanoparticles were of a

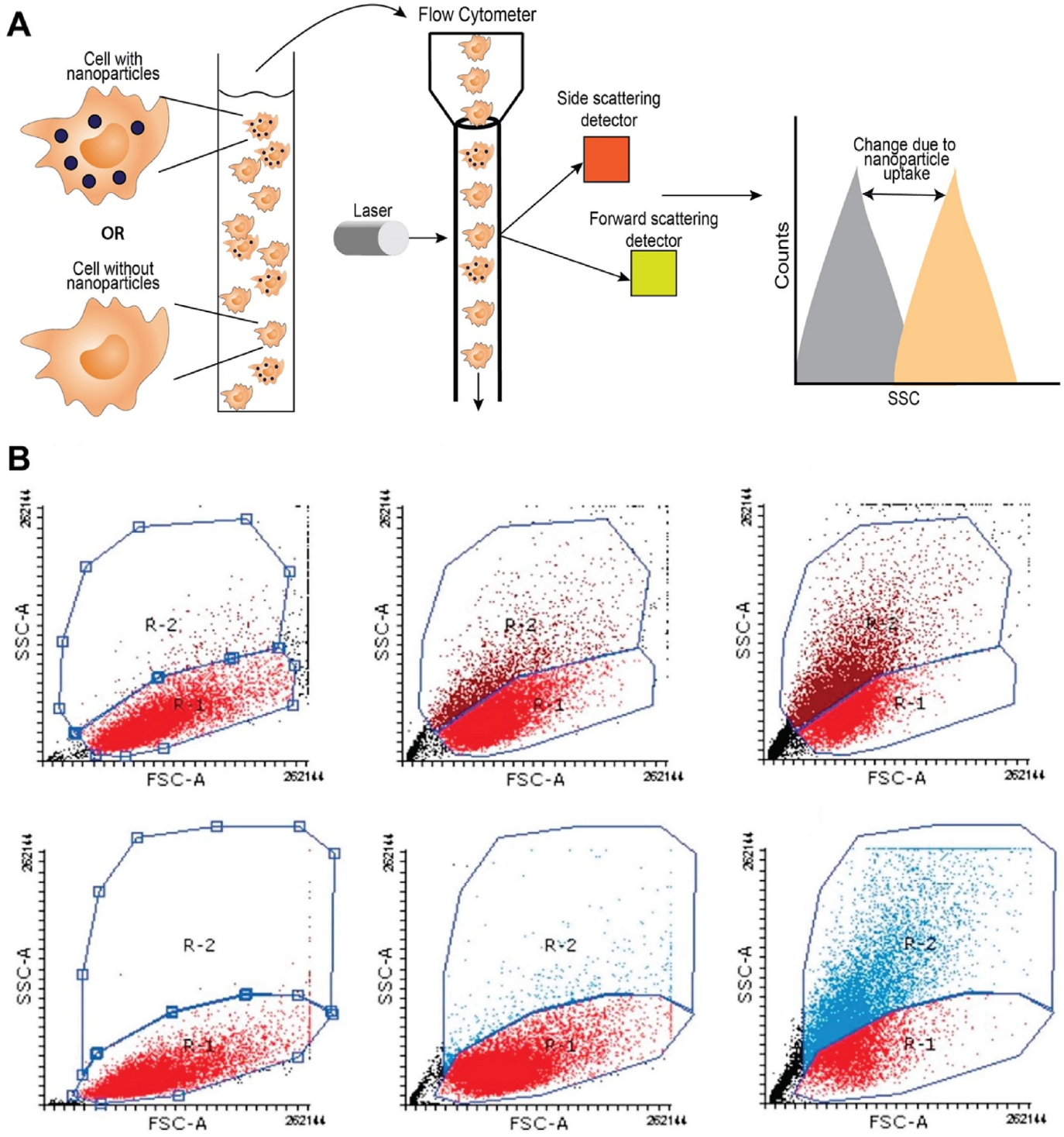

Fig. 1. Flow cytometry for label-free quantification of nanoparticle-cell interactions. (A) A schematic overview of the sample introduction and measurement workflows. A single-cell suspension is run through the flow cytometer. At the interrogation point, data is collected and a histogram showing the count vs side scattering is generated. The side scattering values increase with the magnitude of nanoparticle interactions with cells. **(B)** PC3 cells (top line) and BPH1 cells (bottom lines) were exposed to magnetite nanoparticle at concentrations of 0, 100 and 500 $\frac{\mu g}{mL}$ (left to right), and nanoparticles were detected in a label-free way using flow cytometry-based measurements of side scattering signal and forward scattering signal. Adapted with permission from Ref. [36]. Copyright 2023 Journal of Magnetism and Magnetic Materials.

smaller size than that of the ZnO nanoparticles.

The ability of conventional flow cytometry to identify and quantify individual cells, while gaining insight into nanoparticle interactions with cells, does come with some notable limitations. Firstly, the number of fluorescent channels in a conventional flow cytometer is limited due to spectral overlaps of fluorophores, limiting the ability to quantify complex cellular phenotypes, as needed for many immunological studies [22,70]. If not specifically combined with an imaging system, it is challenging to get spatio-temporal information from single cells in a high throughput

manner using conventional flow cytometry [71]. The lack of imaging further complicates identification and resolution of coincidental events, where multiple cells interact with the laser simultaneously. Conventional flow cytometry is further prone to some ambiguity in results, as cell debris or nanoparticle aggregates will be detected alongside whole cells [72,73]. Careful selection of appropriate control groups and tools, such as gating strategies and scattering signal threshold settings, are needed to address this limitation [73]. Moreover, quantifying protein abundance from raw fluorescence signals remains challenging with conventional flow cytometry. Finally, antibody labeling is challenging for some cells or cell markers, complicating the analysis of specific cell lines [74].

Recent innovative contributions have aimed to overcome some of the limitations of conventional flow cytometry. For instance, the implementation of microfluidics-based cytometry, which uses a microchannel with a microfabricated window for detecting fluorescence signals, enables cell characterization and detection of intracellular proteins [75]. Cells tagged with fluorescent dye-labeled antibodies can pass through the microchannel to evaluate and quantify fluorescence emission intensity. Additionally, this method allows for quantification of cell diameter and the absolute number of proteins and associated protein concentration at the single-cell level, as demonstrated by Li et al. The researchers quantified the number of β-actin proteins on A549 human lung cancer cells, Hep G2 human liver cancer cells, MCF 10 non-tumorigenic human breast epithelial cells, and HeLa human cancer cells. Although this study did not quantify nano-bio interactions, it is worth noting that this study can be improved upon to characterize proteins, such as p53, at the single-cell level to allow for the study of tumor heterogeneity and nano-bio interactions through examining the effect of nanoparticles on cancer cells [75].

Spectral analyzer technologies have been applied to conventional flow cytometers, creating a spectral fingerprint that measures the full fluorescence emission spectra in multicolor samples for each individual fluorochrome. Each spectrum is isolated for precise signal determination [22,76,77]. Furthermore, a spectral analyzer allows for the analysis of up to 48 channels, thus substantially expanding the analysis capabilities of conventional flow cytometers [76].

RNA flow cytometry, which facilitates the detection of multiple RNA transcripts with high sensitivity from single cells in heterogeneous samples, has also demonstrated significant promise [78]. RNA flow cytometry utilizes RNA expression as an identifier, particularly in cases where antibodies cannot be used to label the cells of interest. Additionally, RNA flow cytometry allows for analyzing gene expression through the detection of fluorescent tags attached to the cell targets. Correlation between mRNA transcripts and antigen expression of tagged cell proteins can be made at the single-cell level, allowing for analysis of metabolic profile, cell type, or cell stage [74,79]. New developments have been made in which techniques such as simultaneous quantification of protein expression and multiple mRNA transcripts at the single cell level can occur [80–82]. This simultaneous analysis allows for the correlation of mRNA with changes in cellular proteins at the single-cell level.

2.2. Spectral flow cytometry

Spectral flow cytometry improves upon conventional flow cytometry by using an optical filter-based division multiplexer to disperse emitted light across sensitive arrays of photodiodes [83,84]. Typically, spectral flow cytometry has been used to analyze high-abundance proteins on cells for immunophenotyping [77,85,86].

Recently, the technology has been improved upon through methods that decrease probing volume and increase the exposure time of each particle in the cell sample to the laser, improving photon generation and minimizing background signal [84]. These changes have been implemented through the creation of spectral nano-flow cytometry (nFCM), which allows for the detection of nanoparticles interactions with cells, with particles as small as 7 nm being successfully detected [84,87–90]. nFCM has been reported to be 4–6 orders of magnitude more sensitive in detecting side scattering signal and 1–2 orders of magnitude more sensitive in fluorescence emission detection compared to conventional flow cytometry [91]. The increased sensitivity of nFCM is attributed to significant background signal reduction and an increased spectral resolution of 2.1 nm [84,92]. The increased spectral resolution of nFCM is made possible by the holographic grating that rejects out-of-focus scattering signals and ensures that the photons are dispersed according to wavelength [84,93].

A study by Li et al. used nFCM to quantify biotinylated *E. Coli* labeled with different quantum dot (QD) streptavidin conjugates, i.e., QD525, QD565, QD605, QD655, and QD705. nFCM was needed for this study to effectively resolve between the different side scattering signals obtained from the five different QDs used. The results demonstrated an increase in spectral intensity associated with each of the quantum dots bound to specific bacterial antigens, allowing for the identification of differing antigen-presenting bacterial cells through nanoparticle labeling [84].

Given its sensitivity, nFCM has been instrumental in studies investigating extracellular vesicles (EVs) [94]. These EVs can be extracted from platelet-free plasma or derived from cells, such as HCT15 human colon adenocarcinoma cancer cells [94]. EVs can be tagged with fluorophore-conjugated antibodies, and their associated fluorescence emission can be detected by nFCM. The interest in EVs stems from their utility as RNA delivery vehicles or as immunosuppression agents. Choi et al. assessed differences in rates of nanoparticle-cell interactions in A431 human epidermoid cancer cells. A431 cells were incubated with extracellular vesicles (EVs) that were derived from these cells and were then analyzed using nFCM to understand the EV populations interacting with the A431 human cancer cells. The data showed a highly heterogeneous distribution of some elements of the EVs, such as surface protein receptors, among all analyzed cells [95].

2.3. Imaging flow cytometry

To allow for visualization of cells as they are analyzed during flow cytometry, imaging flow cytometry has become a recent focus of flow cytometry investigations. Imaging flow cytometry combines conventional flow cytometry with fluorescence microscopy such that cell features can be imaged and spatially resolved during data collection [96–98]. In imaging flow cytometry, cells are imaged using either a traditional CCD camera or a photomultiplier (PMT) method as they flow through the microfluidic channels leading to the laser (Fig. 2A–C) [99]. 2D imaging allows for cell phenotyping by visualizing the cells' physical characteristics. Imaging data can be obtained when a laser beam interacts with individual cells in the flow tank. This interaction can then get processed and digitized through appropriate microscope objective lenses as well as flow cytometric lenses and filters [100,101]. In addition to the images, traditional flow cytometry light scattering signal data can be obtained [99,102]. The imaging capabilities of imaging flow cytometry allow for the detection of cell movement as well as the colocalization of nanoparticles within cells [103]. It is necessary that users understand the complexity of the sample and sample environment to determine which imaging flow cytometry approach, camera-based or PMT based method, best suits their needs [100,101].

Recent studies with imaging flow cytometry have been performed with white blood cells to classify them by type, rather than

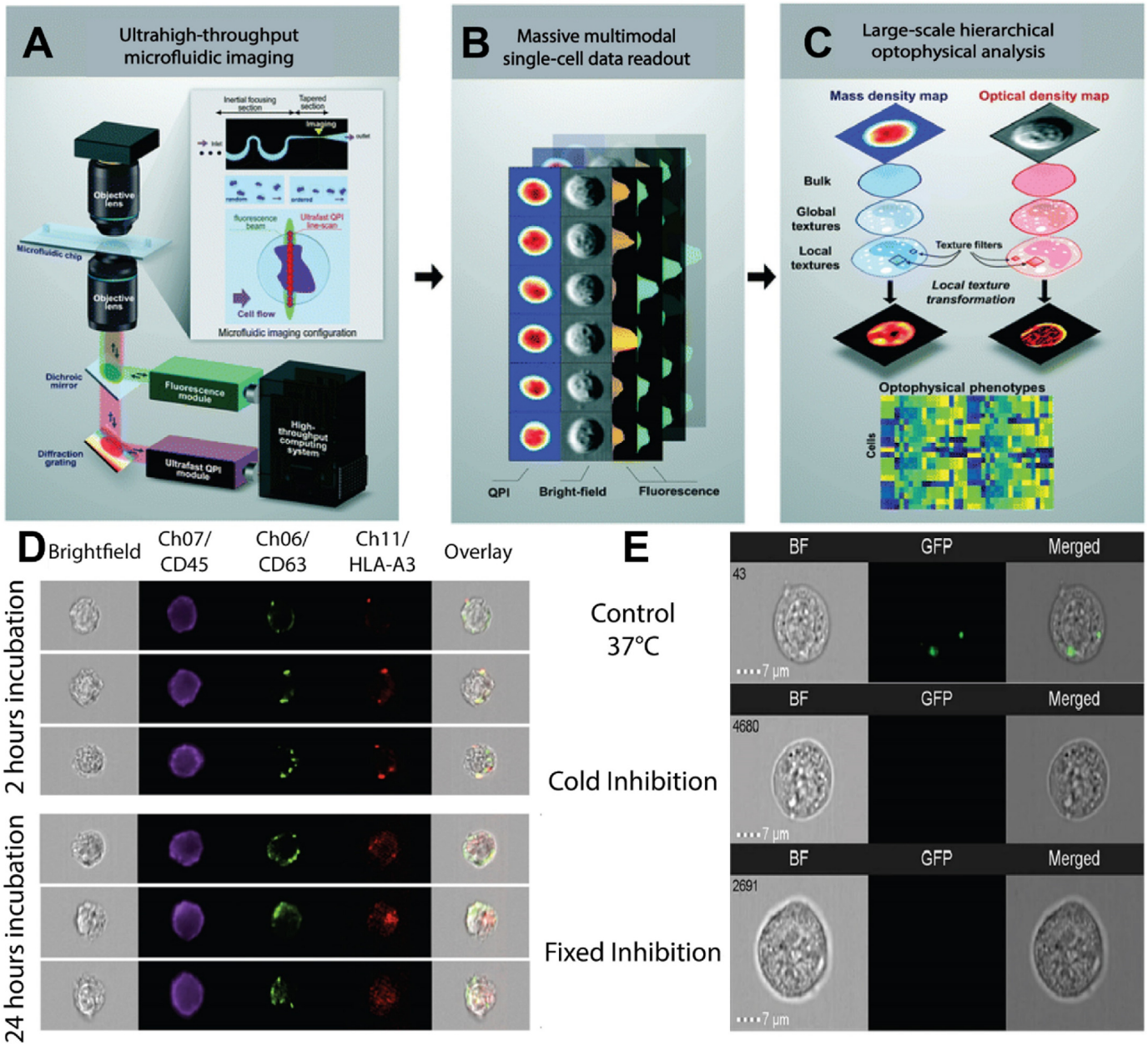

Fig. 2. Imaging flow cytometry workflow and data of nanoparticle-cell interaction. **(A)** The general workflow of an imaging flow cytometer. A fluorescence and a quantitative phase image (QPI) module are used for image acquisition of the sample flowing through the microfluidic chip. **(B)** Once the sample is run through and the cells have been aligned through the chip's single stream, 2D images of single cells in suspension are reconstructed. **(C)** Once the images are reconstructed, they are used for analyses that integrate the correlation between different cell-type classifications. Reproduced with permission from Ref. [99]. Copyright 2023 Lab on a Chip. **(D)** Using a similar workflow, images of HLA-A3 human cells were incubated with extracellular vesicles for various periods of time, i.e., 2 h vs. 24 h. Images of the different conditions are shown. Reproduced with permission from Ref. [116]. **(E)** Representative imaging flow cytometry images of HEK293T extracellular vesicle interactions with HEK293T human cells at different conditions, i.e., at 37 °C, 4 °C. Reproduced with permission from Ref. [117]. Copyright 2023 Springer Nature.

solely by cell cycle [104,105]. Imaging flow cytometry has also been used to assess nano-bio interactions. For example, Vranic et al. used imaging flow cytometry to identify the time- and dose-dependence of TiO_2 and SiO_2 nanoparticle interactions with NCI−H292 human pulmonary epithelial cancer cells. During this analysis, the researchers discovered that the endocytosis pathway for SiO_2 was micropinocytosis through visually tracking cell features following endocytosis pathway inhibition and nanoparticle treatment [45]. Interestingly, a majority of recent imaging flow cytometry studies have focused on the analysis of extracellular vesicle interactions with cells, and the delivery of EVs to cells (Fig. 2D−E) [48,72,106−111]. We attribute this trend to the growing interest in the use of EVs for therapeutic cargo delivery and the assessment of cellular senescence and aging [112−115]. For instance, Görgens et al. analyzed the interactions of EVs and small EVs that were derived from THP-1 human cancer cells with THP-1 cells after labeling the EVs with CD63eGFP. The researchers reported that EVs and small EVs could also be detected in unprocessed samples. Their findings, therefore, will allow for an easier analysis of EVs and their interaction with cells without the need to isolate the EVs from cells.

Imaging flow cytometry does have its limitations. The cell sorting capability of imaging flow cytometry sorting capability is

very limited. This is because creating an image-based cell sorter requires major enhancements in high-speed image acquisition, as well as the need to incorporate microscale sorting modules and intelligent data analysis methods [102,118–120]. Moreover, it is not feasible to reimage the same cell, as it would be if the cells were imaged using time-lapse slide-based microscopy. This limitation denies the possibility of implementing 3D reconstruction of cells or confocal sectioning (i.e., z-stacking). In addition, there is a lack of workflow automation in imaging flow cytometry. This can lead to significant challenges in downstream analyses as, for example, dozens of masks need to be applied to cellular objects and subcellular compartments for complete analysis [102]. Tracking of cell samples as they flow through the microfluidic chamber for temporal snapshot analysis has yet to be achieved [102]. Finally, imaging flow cytometry data analysis is intensive, requiring manual inspection of images coinciding with scattering data. Scaling experiments to align with reasonable data analysis approaches remains a challenge in imaging flow cytometry methods.

Even with these challenges, imaging flow cytometry advantages are multifold. Imaging flow cytometry uses a sensitive CCD camera that allows for the identification of pixels that have higher signals than their surroundings and provides a better resolution than that of conventional flow cytometry [48]. Additionally, with the imaging processing tools available for imaging flow cytometry, identification of coincidental data is possible, a phenomenon unattainable with conventional flow cytometry [110]. Furthermore, in terms of extracellular vesicle analysis, the slower flow rate of imaging flow cytometry paired with CCD-camera based detection allows for a more effective extracellular vesicle analysis platform compared to conventional flow cytometry [108]. It is also worth noting that imaging flow cytometry instruments have low background, an increased fluorescence sensitivity, and great data analysis tools that can incorporate machine learning algorithms [72].

Beyond these advantages, recent developments in imaging flow cytometry have sought to overcome the previously discussed challenges. For example, studies using digital holography have generated tomographic flow cytometry, allowing for collection of 3D information of target particles [121–123]. Recent studies have aimed to develop machine and deep learning algorithms to train models for evaluating and classifying imaging flow cytometry images (Fig. 3), providing improved analysis workflows [104,124,125]. Also, future improvements can be done to remove the snapshot limitations, in which images of the cell sample are taken as the cell passes specific points in the microfluidic channel, and implement object or sample tracking [102,122,126]. It is worth noting that a virtual-freezing fluorescence imaging flow cytometry method has been developed to allow for a longer exposure time for image acquisition, thus, facilitating high-throughput imaging flow cytometry of >10,000 single cells per second without losing spatial resolution or sensitivity [127].

2.4. Photoacoustic flow cytometry

Conventional flow cytometry approaches have been paired with photoacoustic technology to produce photoacoustic flow cytometry (PAFC) and photoacoustic imaging flow cytometry [49]. The PAFC system is comprised of five main components: a transducer, a laser, a microscope, a flow tank, and a pump system (Fig. 4A–C) [50,128]. The pump system shuttles cells into a capillary tube where the cells are irradiated by a laser. The cells absorb laser light and generate an acoustic wave that is detectable by the transducer. The microscope correlates the firing rate of the laser and the sample passage with the acoustic signal recorded by the transducer. Transducer signals are sent to an ultrasound receiver, where they are amplified for data collection. Scanners can be implemented to record images of cells as they move through the microfluidic systems [53].

Specifically, a diode-pumped pulsed laser is used for photoacoustic (PA) excitation. Once excited, the acoustic waves are collected and separated from the excitation light using dichroic mirrors and bandpass filters. The transducer then detects photoacoustic events in the flow chamber [53,129]. The intensity of the collected photoacoustic signal is then measured using a photomultiplier tube connected to a high-voltage pre-amplifier. The PA signals are then amplified and digitized. Recorded amplitudes of PA signals along with voltage signals from the photomultiplier tube are recorded and compared [51], which is possible due to the setup of the flow chamber allowing for the collection of excitation and acoustic waves [130].

PAFC has been used to characterize nanoparticle interactions with cells. Nedosekin et al. quantified interactions of antibody-labeled gold nanorods with MDA-MD-231-GFP human and ZR-57-1 human breast cancer cells, whereby photoacoustic signal from cells treated with the gold nanorods increased by nearly two orders of magnitude compared to controls [51]. Cells labeled with nanoparticles have also been observed using PAFC, such as in a study by Bhattacharyya et al. where T47D breast cancer cells were labeled with fluorescent latex nanoparticles [52]. Sun et al. used multiparametric PAFC (MPAFC) to successfully identify three different cell lines – 9 L mouse cells, HeLa cervical cancer cells, and C6 mouse cells – labeled with three different polymer nanoparticles in simulated blood while, eliminating cross-labeled or label-free cells from analysis (Fig. 4D) [53].

PAFC is capable of detecting nanoparticles at a high sensitivity and characterizing cells without compromising the light scattering and fluorescence detection of various biomarkers. However, PAFC can experience deterioration of imaging power due to a majority of suspended cells being distributed out of the focal plane as a result of limited axial resolution and depth of field [45,51]. However, these limitations can be overcome by the introduction of an acoustic standing wave, which helps confine the suspension cells to the focal plane of the illumination, thus avoiding any effect from the limited axial resolution and depth of field [53]. Implementation of point-to-point scanning can lead to a low throughput and decreased imaging speed. Moreover, the wavelengths of lasers with high pulse repetition rates are restricted, meaning only an exclusive selection of chromophores can be distinguished by the two-color illumination scheme [53,131].

Innovation in PAFC has produced promising advancements. PAFC analysis speed can be significantly increased as data processing algorithms are implemented [78]. PAFC has also been used for *in vivo* sample analysis, where the organism's body is used as the medium in place of a flow tank or pump system [132–134]. Flow cytometry techniques are generally limited in *ex vivo* analysis, for example demonstrating low sensitivity while detecting circulating tumor cells, in addition to requiring intensive sample preparation and data analysis methods [78,135]. Using *in vivo* flow cytometry via PAFC has allowed for the detection of fluorescently labeled low abundance circulating tumor cells directly in the blood of mice [136]. For instance, Yao et al. used *in* vivo flow cytometry to study the ability of nanoparticles to target circulating tumor cells. The authors found that fluorescently labeled polymer nanoparticles coated with neutrophil members could more efficiently target circulating tumor cells compared to uncoated nanoparticles [60]. Several studies have used similar *in vivo* approaches to assess how nanoparticles affect blood flow and cells in the blood, such as circulating tumor cells and melanoma cells [52,54,57,61].

3. Elemental analysis and mass spectrometry

Direct analysis of individual elementals is a powerful tool for

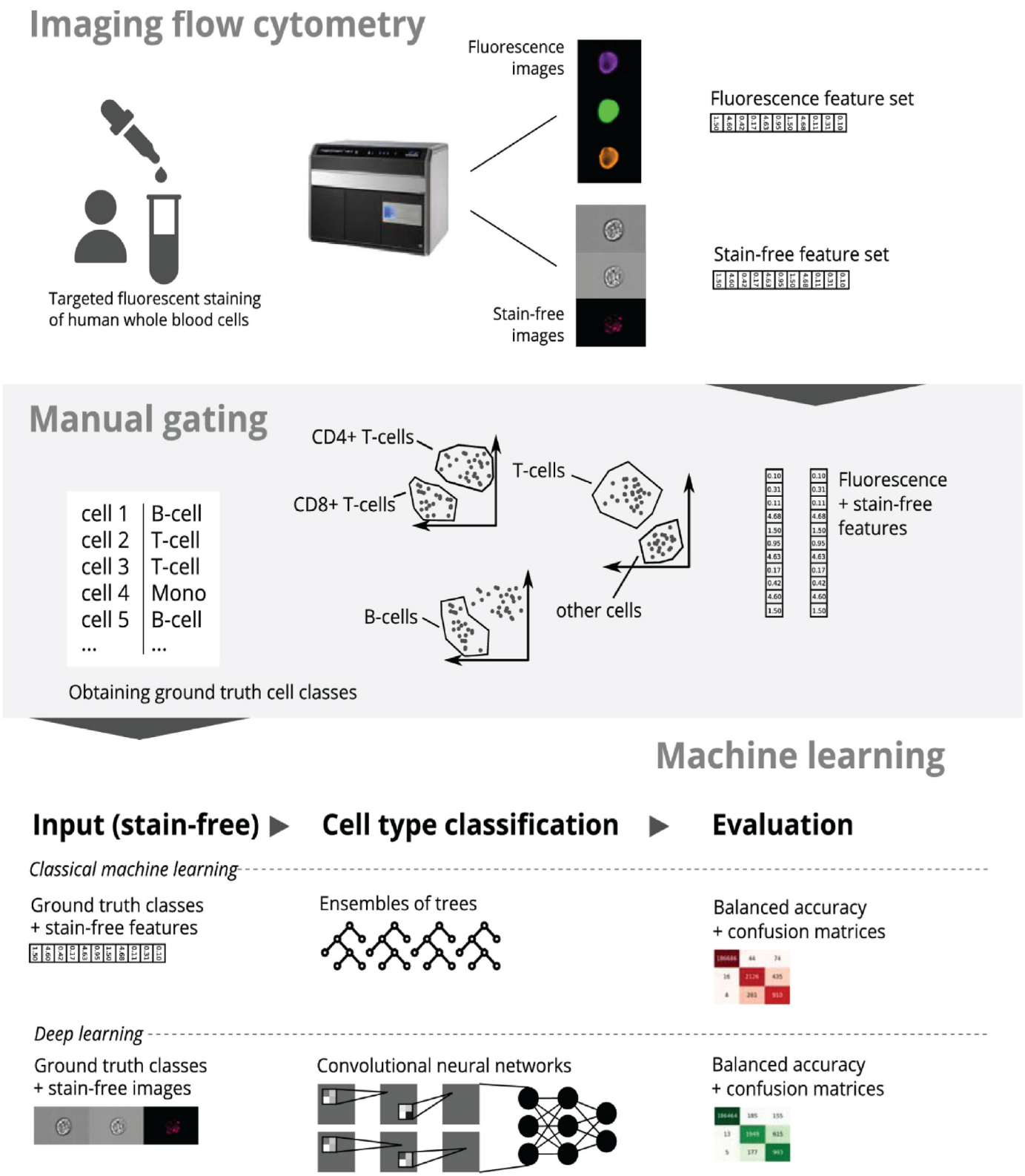

Fig. 3. Data processing techniques for imaging flow cytometry. Machine learning algorithms and deep learning models are utilized for the evaluation and classification white blood samples from healthy donors. Reproduced with permission from Ref. [104]. Copyright 2023 Cytometry Part A.

quantifying nanoparticle-cell interactions. Cells possess endogenous elemental fingerprints that can be used to identify cells compared to background signals. Additionally, exogenous staining or labeling agents can be used to identify cells using high atomic weight isotopes (i.e., Ir, Y, etc.). Nanoparticles comprised of inorganic elements or tagged with elemental markers can be identified and quantified. Quantifying the amount of each element in cell samples exposed to elemental labeling agents or nanoparticles

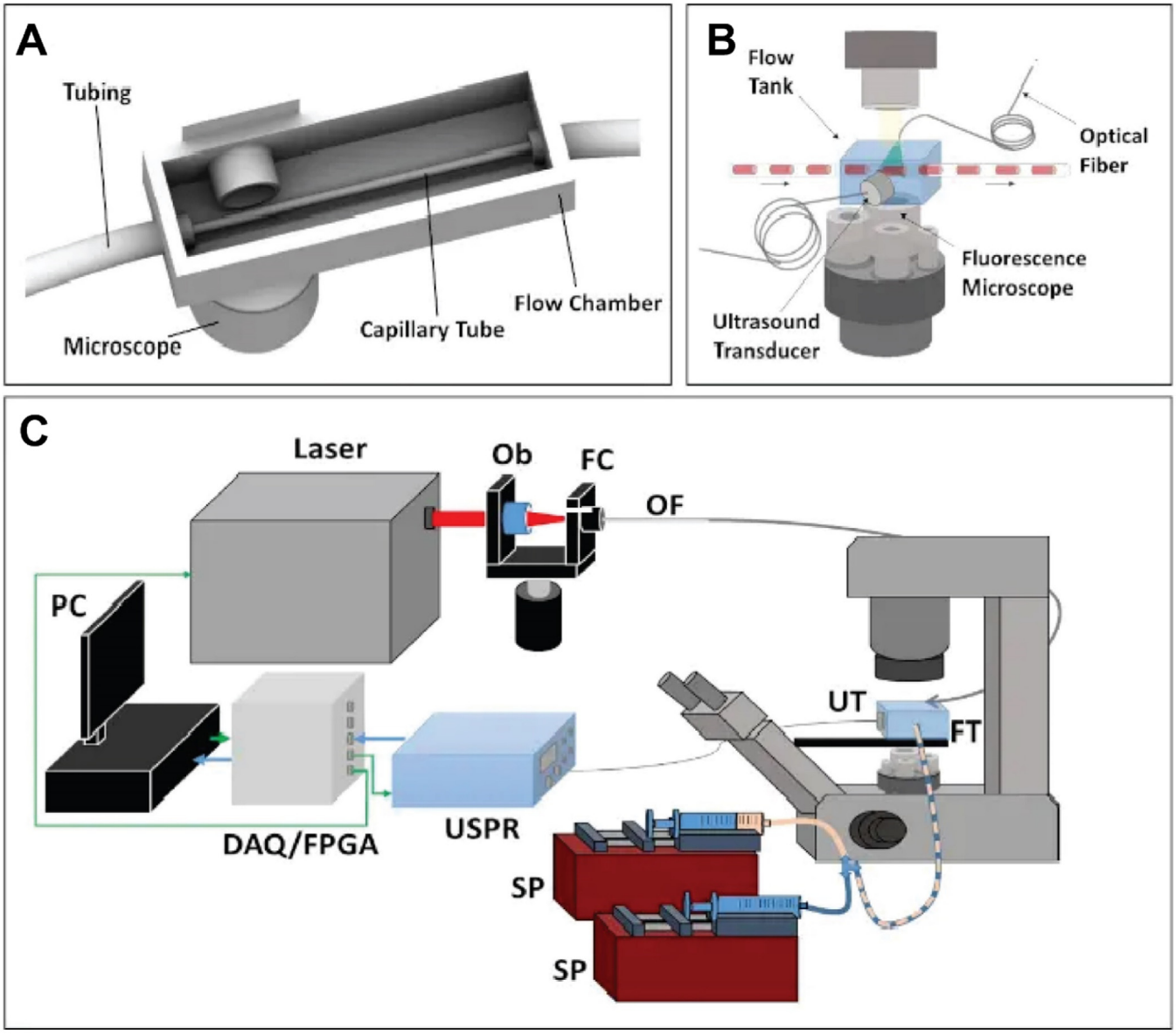
A
Tubing
Microscope
Capillary Tube
Flow Chamber
B
Flow
Tank
Optical
Fiber
Fluorescence
Microscope
Ultrasound
Transducer
C
Laser
Ob
FC
OF
PC
UT
FT
USPR
DAQ/FPGA
SP
SP
D
Tumor cell-CNPPV
Tumor cell-BDT-TQE
Tumor cell-SP2
Blood cell
Melanoma cell
i
532 nm
ii
770 nm
iii
30 μm

allows for accurate quantification of nanoparticle interactions with cells and can be used to identify cell phenotype. While multiple tools can be used for elemental quantification, one of the most used and effective methods is inductively coupled plasma mass spectrometry (ICP-MS). Here, samples are atomized and ionized by an argon plasma and the resulting ion cloud is focused and filtered through transmitting ion lenses for quantification of desired ions [137]. The high throughput capabilities of ICP-MS technology allow for hundreds of cells to be quantified per minute. When paired with the sensitivity of the technology, trace amounts of elemental signal can be detected and quantified with appropriate calibration [138]. These characteristics of ICP-MS paired with recent advances in the field propel ICP-MS technology to the forefront of effective means of quantifying nanoparticle-cell interactions at the single-nanoparticle and single-cell level.

3.1. Quadrupole ICP-MS

The most widely used iteration of ICP-MS instruments is quadrupole ICP-MS (ICP-Q-MS). ICP-Q-MS uses a quadrupole to filter out undesired ions, permitting accurate detection and quantification of a single specific ion [137]. ICP-Q-MS has been used to quantify nanoparticle-cell interactions in multiple studies, though many of these approaches require destruction of cell samples through acidification [139–142]. Further, the resulting data only provides mean population data that fails to reach the ideal of single-nanoparticle and single-cell resolution. Single particle ICP-Q-MS (SP-ICP-Q-MS) approaches provide avenues for quantifying elements one cell at a time through using alternative hardware compared to traditional ICP-Q-MS. SP-ICP-Q-MS has been used to quantify cellular uptake of gold [24,143,144], silver [145–147], and platinum [148] nanoparticles in varying cells lines, as shown in Table 2. In each case, the presence and number of nanoparticles in cells could be accurately identified, providing insight into nanoparticle-cell interactions at the single-cell level. SP-ICP-Q-MS has also been used to quantify elements intrinsic to themselves, such as copper and zinc [149].

Introduction of single cells into the instrument is a key consideration when assessing measurement of individual cells. SP-ICP-Q-MS does not possess innate methods for visualizing or identifying cell entry into the instrument, relying solely upon exogenous or endogenous elemental signal detection and analysis to identify cell entry and measurement. Additionally, sample introduction methods do not delivery cells with 100% transport efficiency and may also introduce opportunity for multi-cell event quantification. Recent innovative methods for improving and tracking introduction of single cells for ICP-MS analysis include microfluidic control mechanisms, magnets, and cameras to visualize individual cell entry into the instrument [150–153].

Another method to ensure measured signal aligns with single cells is to count cells through cell-associated elemental analysis. Based on quadrupole settings and short transient ion signals from cells and nanoparticles, SP-ICP-Q-MS on its own is only capable of accurately measuring one element at a time [137,149]. While quantifying a single element allows for label-free cellular quantification, this single-element quantification approach is also a limitation that prevents simultaneous quantification of both cell-associated or cell-labeling elements and nanoparticles [25].

Recent studies have overcome this limitation using dual-analyte techniques, whereby the transient ion cloud resulting from ionization at the plasma torch is stretched using collision gases, such as NH_3 (Fig. 5A) [154–156]. This ion cloud stretching provides ample time for quadrupole switching to occur within the same event (i.e., particle), allowing for two elements to be measured for each sample. Donahue et al. used this approach to quantify gold nanoparticle uptake in nonadherent Raji B cells. After incubation with gold nanoparticles conjugated to peptides that increase cellular uptake, the cells were labeled with ^{114}Cd quantum dots and fixed using paraformaldehyde. Dual-analyte SP-ICP-Q-MS was then used to measure both ^{197}Au and ^{114}Cd simultaneously, so both gold nanoparticles and cells could be quantified by ^{197}Au and ^{114}Cd, respectively (Fig. 5B–D) [25]. In this study, ^{114}Cd quantum dot labeling was used instead of more traditionally applied ^{193}Ir labeling due to the weak ^{193}Ir signal intensity measured using dual-analyte methods, demonstrating that this method reduces signal intensity and, thus, influences the limit of detection. By using dual-analyte SP-ICP-Q-MS approaches, simultaneous tracking of cells and nanoparticles is made possible, expanding upon current SP-ICP-Q-MS options for understanding nanoparticle-cell interactions.

3.2. Laser ablation ICP-MS

Traditionally, ICP-Q-MS measurements are performed using aqueous solutions or with samples suspended in solution (i.e., non-adherent cells). Adherent or dried cells can be quantified using laser ablation ICP-MS approaches (LA-ICP-MS), whereby individual cells can be ablated with a laser and the resulting aerosol is carried to the ICP-MS for quantification [157]. Previous studies have used this technique to quantify metallodrugs, such as cisplatin, in cell and tissue samples following treatments [158–162]. Nanoparticle uptake in cells and tissues has also been measured using LA-ICP-MS [163–165].

Historically, challenges with LA-ICP-MS single cell analysis include ablating individual cells, comparing ablated signal against appropriate standards, and low throughput of LA-ICP-MS methods. Recent studies have aimed to overcome these issues using novel approaches for arraying individual cells inside of droplets containing known concentrations of ionic standards. One study by Zheng et al. used microfluidic channels to flow RAW 264.7 murine macrophages treated with silver nanoparticles through a PDMS mold containing evenly spaced “traps” to capture individual cells, which then adhere to the surface of the dish (Fig. 6A–C). After the mold was removed (Fig. 6D), an inkjet printer dispensed a droplet of known ion concentration onto each individual cell (Fig. 6E) before the cells were quantified by LA-ICP-MS (Fig. 6F–I). LA-ICP-MS results for nanoparticle uptake matched those observed from standard ICP-Q-MS quantification [166]. Similar cell array and doped droplet approaches have been used with ICP-Q-MS [167] and time-of-flight ICP-MS analysis [168].

3.3. Time-of-flight ICP-MS

Another approach for ICP-MS elemental quantification uses time-of-flight methods (TOF-ICP-MS). Here, the transient ion signal

Fig. 4. Photoacoustic imaging flow cytometry (PAIFC) for the identification of nanoparticle interactions with cells. **(A)** Diagram of the different components of a photoacoustic imaging flow cytometer. The single cell sample flows through the flow chamber. **(B)** Components of the photoacoustic flow cytometer system. **(C)** The components of a PAIFC system. SP = syringe pump; DAQ/FPGA = data acquisition/field programmable gate array; Ob = objective lens; OF = optical fiber; FC = fiber coupler; UT = ultrasound transducer; FT = flow tank. Adapted with permission from Ref. [49]. Copyright 2023 Journal of Visualized Experiments. **(D)** Multiparametric photoacoustic flow cytometer is used to analyze C6 (green), HeLa (blue), and 9 L (orange) cells that were labeled with SP2, BDT-TQE, and CNPPV polymer nanoparticles, respectively, is shown. The maximum amplitude projection (MAP) images of labeled tumor cells at **(i)** 532 and **(ii)** 770 nm respectively. **(iii)** The PAIFC could identify the cells using the photoacoustic wavelengths generated by each cell Adapted with permission from Ref. [53]. Copyright 2023 American Chemical Society.

Table 2
Summary of single-cell studies using ICP-MS instrumentation.

Instrument	Cell (Label) Elements	Nanoparticle Elements	Cell Line(s)	Notable Methodology	References
SP-ICP-Q-MS	None	^{197}Au	Human T24	As few as one PEGylated gold nanoparticle could be detected per cancer cell.	[24]
	None	^{197}Au	*Cyptomonas ovate*	Gold nanoparticle uptake measured in algal cells	[144]
	^{63}Cu,^{64}Zn	^{197}Au	CP70, A2780, CAOV3	*Distinct* quantification of gold nanoparticle uptake and cell ionic signal	[149]
	None	^{197}Au	MDAMB231, T47D	Detailed computations and correlation of nanoparticles with electron microscopy	[143]
	^{114}Cd (label)	^{197}Au	Raji B Cells	Dual-analyte detection through ion-cloud stretching by collision gases (NH_3)	[25]
LA-ICP-Q-MS	^{31}P	^{107}Ag,^{109}Ag	RAW 264.7	Cellular array for individual cell ablation	[166]
	^{31}P	^{107}Ag,^{109}Ag	16HBE human normal bronchial epithelial cells	Cellular array for individual cell ablation	[167]
LA-TOF-ICP-MS	^{23}Na,^{24}Mg,^{31}P,^{66}Zn,^{191}Ir (label),^{193}Ir (label)	None	THP-1	Cellular array for individual cell ablation, quantification of multiple endogenous cellular elements	[168]
TOF-ICP-MS	^{24}Mg,^{31}P	^{197}Au,^{138}Ba	*Raphidocelis subcapitata*	Simultaneous detection of multiple endogenous cell and exogenous nanoparticle elements	[175]
CyTOF	^{191}Ir (label)	^{109}Ag	THP-1	Silver nanoparticles used during calibration to improve nanoparticle quantification	[181]
	^{191}Ir,^{193}Ir (label)	^{107}Ag,^{109}Ag	TIB-152	Ir staining of cells prior to nanoparticle treatment	[182]
	^{191}Ir (label)	^{107}Ag	Jurkat	Ir staining, results compared to traditional ICP-MS and SP-ICP-Q-MS	[183]
	^{147}Sm,^{152}Sm,^{168}Er,^{172}Yb, ^{174}Yb,^{176}Yb, ^{148}Nd,^{142}Nd,^{159}Tb,^{170}Er,^{151}Eu,^{165}Ho,^{191}Ir,^{193}Ir (all labels)	^{197}Au	RAW 264.7, C57BL/6 mouse lymph node tissue	Assessing gold nanoparticle uptake by murine cells and murine cell phenotyping to identify differences in nanoparticle interaction based on cellular identity	[184]

formed during the atomization and ionization of the sample is separated into individual ion signals in a time-of-flight mass analyzer. This separation occurs based on principle differences in the mass-to-charge (i.e., *m/z*) ratio values between ions and allows for the quantification of multiple ions in the same analyzed particle [169]. Additionally, the sensitivity of TOF-ICP-MS allows for the quantification of low atomic weight elements, with carbon having been successfully quantified in polymer beads [170]. This ability allows for cells to be identified and quantified without the need for cell visualization or tracking strategies during sample introduction. Additionally, exogenous labeling or staining agents can be disregarded as the elemental footprint of individual cells themselves can be sufficiently detected [171,172].

Single cell analysis by TOF-ICP-MS remains a relatively new approach and has been mainly applied for environmental analysis rather than biomedical [173,174]. One study by Hendriks et al. used TOF-ICP-MS to assess gold nanoparticle and $BaSO_4$ nanoparticle uptake by algal cells, using magnesium and phosphorus ion signals to identify cells [175]. Signal overlap between nanoparticle ions (^{197}Au or ^{138}Ba) and cell ions (^{24}Mg and ^{31}P) was interpreted as an indication of interactions, such as cell uptake, between cells and nanoparticles. Other applications of TOF-ICP-MS for single-cell analysis are typically applied alongside flow cytometry technologies, as will be discussed in the next section. Continued investigation into the use of TOF-ICP-MS applications for biomedical and nanomedicine applications is encouraged.

Particularly for biological samples, matrix effects can complicate ICP-MS analysis due to the complex composition of biological and cellular media [176,177]. Removing the matrix effects from sample analysis provides greater confidence in the results. One recent development in the field of TOF-ICP-MS is the use of online microdroplets during sample introduction to overcome sample matrix effects (Fig. 7) [178–180]. After nebulization but before atomization and ionization, cells or particles introduced into the instrument are immersed in microdroplets doped with known concentrations of multiple elements, including the element(s) of interest.

Current studies have shown the value of microdroplet approaches for accurately quantifying nanoparticles in varying matrices [178,180]. The translation of this technology to single-cell experiments offers new opportunities for minimizing matrix effects and increasing confidence in collected data. While these approaches could be used with other ICP-MS techniques, TOF-ICP-MS proves to be the best option based on its unique ability to simultaneously quantify multiple elements, from both the sample and the doped microdroplets, at the single-particle level.

4. Mass cytometry

While mass spectrometry and flow cytometry are independently valuable in quantifying nanoparticle-cell interactions, combining the two techniques affords additional analysis opportunities. Mass cytometry, commonly referred to as cytometry by time-of-flight (CyTOF), combines elemental time-of-flight aspects of mass spectrometry with flow cytometry techniques to identify cells in heterogenous mixtures and subsequently quantify differences in, for example, nanoparticle uptake (Fig. 8A) [184,185]. Since fluorophore emission spectra can overlap, it is preferable to tag antibodies with heavy metal ions rather than with fluorochromes [185–187].

CyTOF instruments do not function in the same way as conventional flow cytometers as they do not have forward scattering signal or side scattering signal light detection or fluorescence signal detection [22]. CyTOF can discriminate between isotopes of various atomic masses with high accuracy; instead of coupling cell-labeling probes (i.e., antibodies) to fluorophores, CyTOF uses probes that are

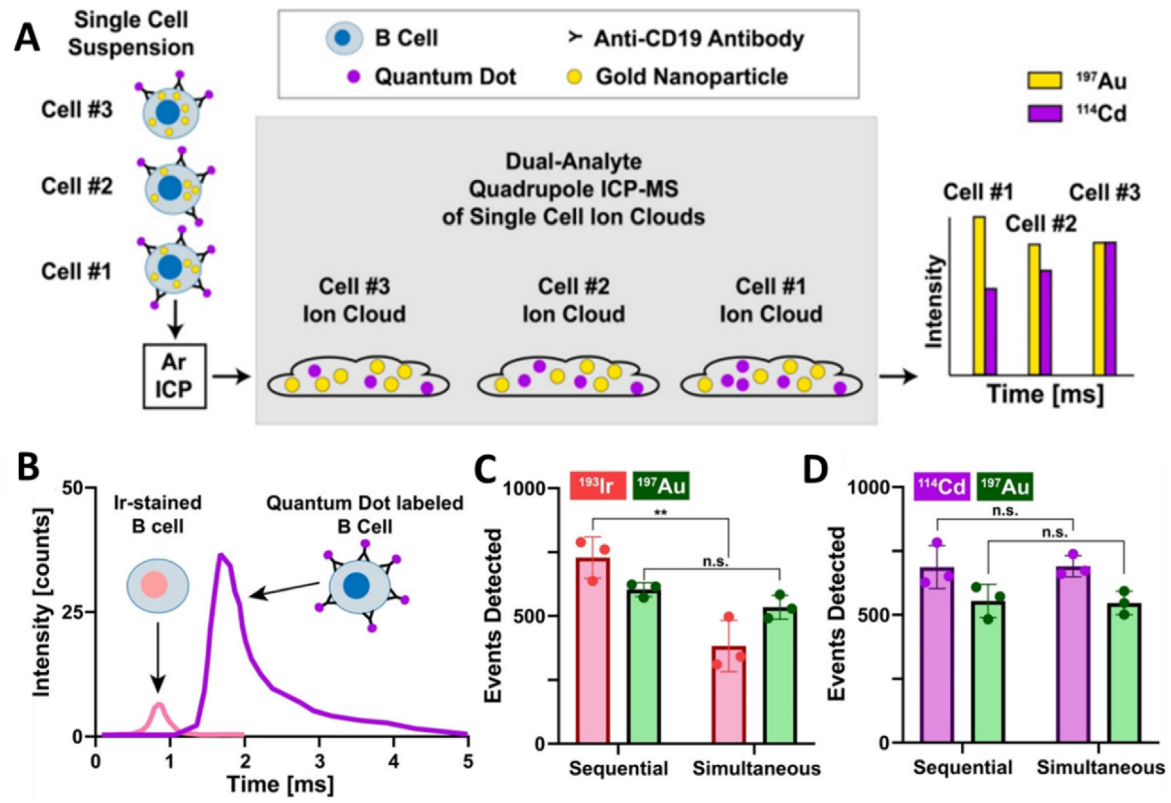

Fig. 5. SP-ICP-Q-MS analysis of two elements in single cells using dual-analyte ICP-Q-MS techniques. **(A)** Schematic overview of sample introduction and measurement workflow. Ion clouds containing the two ions to be analyzed are stretched using collision gases to allow for simultaneous ion measurements. **(B)** Cells stained with ionic ^{193}Ir possess a different transient ion cloud intensity peak compared to cells labeled with ^{114}Cd-containing quantum dots when dual-analyte ICP-Q-MS conditions are used. **(C)** Counting of AuNP-containing cells stained with ionic ^{193}Ir using sequential or simultaneous (i.e., dual-analyte) operating modes demonstrates a mismatch in accurate cell counting. **(D)** Counting of AuNP-containing cells labeled with ^{114}Cd-containing quantum dots using sequential or simultaneous (i.e., dual-analyte) operating modes demonstrates maintained accuracy in cell counting. Reprinted with permission from Ref. [25]. Copyright 2023 American Chemical Society.

coupled to stable heavy-metal isotopes [185,188]. Cell-labeling probes can be extracellular or intracellular, the latter using primarily iridium (Ir) staining methods. CyTOF allows for the analysis of up to 100 isotopes at one time while performing single cell quantification, greatly expanding the possible range of cell analysis options [78,189]. The wide possibility space for isotopic analysis and corresponding cellular features (i.e., phenotypes) distinguishes CyTOF as an effective tool for quantifying complex samples, such as for immune cell analysis [190,191].

Exogenous heavy metal labeling of cells is required in CyTOF to detect and quantify cells as the mass filters cutoff elements below 80 amu, thus preventing the detection of endogenous cellular elements [192]. This cutoff is primarily set to limit background noise and signal interference, as can come from argon dimers (Ar_2), but also limits endogenous elemental quantification [193]. Additionally, in order for the instrument to obtain sensitivities comparable to those of the fluorophores, ~100 atoms of a given isotope should be bound to each antibody or probe, and multiple probes must be associated with cells for accurate cell detection and quantification. The quantity of the isotopes for a particular mass represents a molecular expression of these isotopes, where a little signal overlap is present [188]. These restrictions also mean that detection of single nanoparticles proves challenging for CyTOF, while nanoparticle aggregates not associated with cells may be detected, resulting in signal confusion [184]. It should be noted that CyTOF studies with nanoparticles can forgo cell labeling as many inorganic nanoparticles qualify as “probes” for the purposes of detecting cells. However, correlating nanoparticle elemental signal with another cell-associated signal is not possible with this methodology.

CyTOF has been used for immunoassays as well as for human blood cell phenotyping [194,195]. Nanoparticle quantification has also been performed using CyTOF, largely to assess immune cell interaction with silver nanoparticles [182,183,196] andgold nanoparticles [184]. One study by Schulz et al. used silver nanoparticles as antigen-labeling agents to quantify antigen presence on peripheral blood leukocytes [197]. Another study by López-Serrano Oliver et al. used silver nanoparticles during instrument calibration prior to quantifying silver nanoparticle uptake by THP-1 cells (Fig. 8B–C) [181]. The results of the study suggest that using nanoparticles during calibration allow for greater accuracy in quantifying nanoparticle association with cells compared to ionic calibrations. Nonspecific interactions between nanoparticles and cells has been quantified using CyTOF. Pichaandi et al. treated KG1a human macrophages, THP-1 cells, and Ramos lymphocytes with different doses of liposome-encapsulated lanthanide nanoparticles. Their results indicated low levels of interaction between the liposome encapsulated nanoparticles and treated cells across different treatment doses and incubation times, demonstrating how CyTOF can quantify nano-bio interactions with low interaction frequency [198]. Finally, in a study by Yang et al., CyTOF has been used to simultaneously perform cell phenotyping of excised C57BL/6 mouse lymph node tissue labeled with a heavy-metal antibody cocktail and treated with gold nanoparticles of varying surface chemistries. Their approach demonstrates the ability of CyTOF to simultaneously identify cell phenotypes and nanoparticle quantification based upon the intensity of isotopic signals [184].

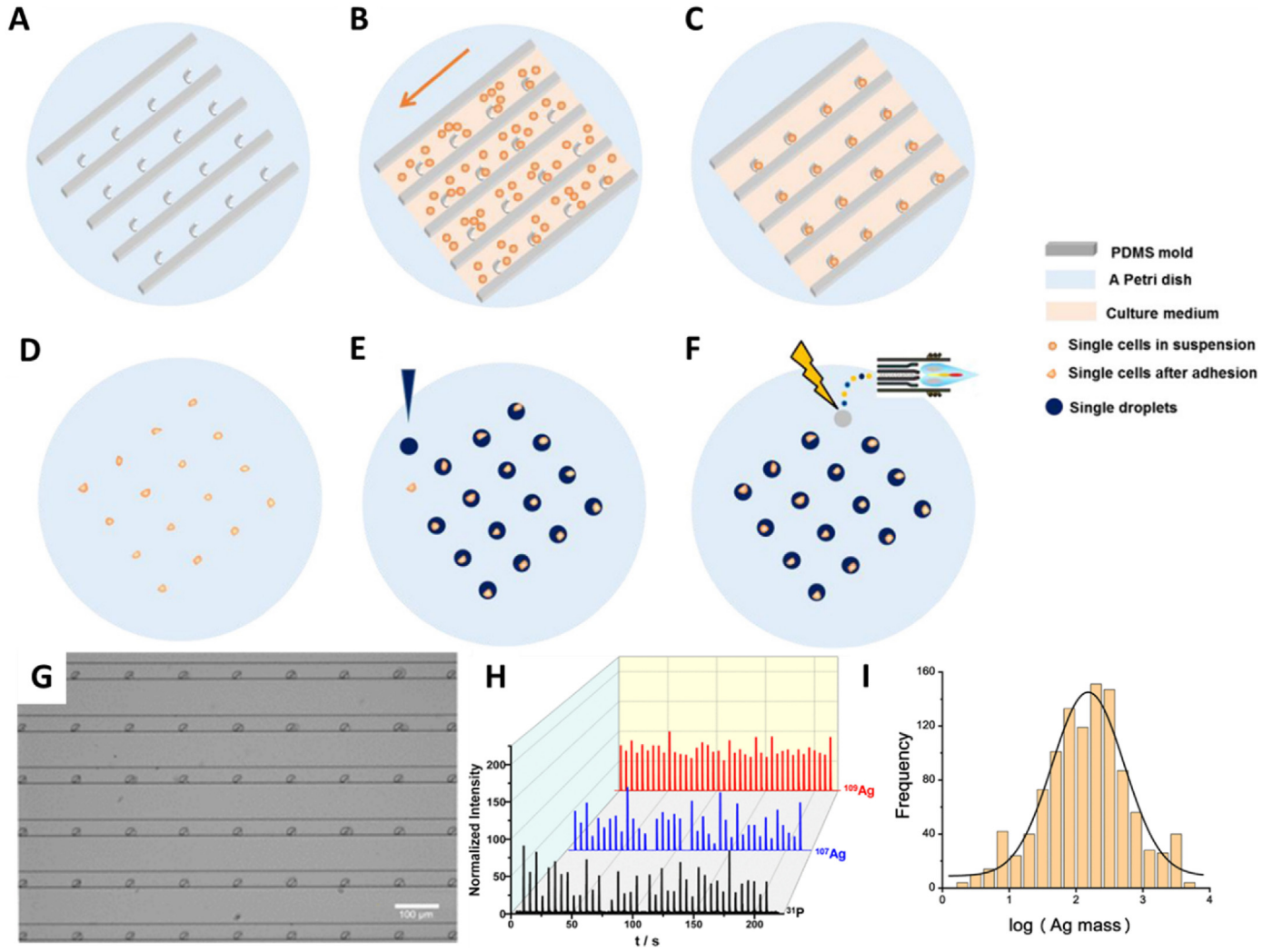

Fig. 6. Arraying single cells for laser ablation ICP-MS analysis. **(A)** A PDMS mold possesses hook-shaped traps to capture individual cells. **(B)** Cells suspended in media flow through the mold, resulting in the capture of individual cells inside the hook-shaped traps. **(C)** Trapped cells are allowed to adhere to the Petri dish where cell capture occurred. **(D)** The PDMS mold is removed, leaving individual cells arrayed on the Petri dish **(E)** Droplets enriched with the ion of interest (i.e., ^{109}Ag). are dropped onto each arrayed cell. **(F)** Each point in the array, containing a single cell inside the ion-enriched droplet, is ablated via laser and quantified by ICP-Q-MS. **(G)** Single cells trapped inside the hook-shaped traps of the PDMS mold can be seen using brightfield microscopy imaging. **(H)** Transient ion signals collected during laser ablation ICP-Q-MS measurements of arrayed single cells treated with AgNPs. **(I)** Quantified Ag content of measured cells. Reproduced with permission from Ref. [166]. Copyright 2023 American Chemical Society.

One recent innovation with CyTOF allows for visualization of cells prior to elemental quantification. Imaging CyTOF uses laser ablation with a small laser spot size to enhance spatial resolution, though at the expense of a reduced sensitivity, due to lower ions being collected from each spot [199,200]. Imaging mass cytometry can be used in genomics to examine the *in vitro* uptake and cellular distribution of DNA. For instance, Malile et al. used DNA-functionalized gold nanoparticles as probes in imaging CyTOF as only picomolar of nanoparticles were required to be used when compared to conventional flow cytometry [201].

To compare mass spectrometry techniques for quantifying nanoparticle-cell interactions, one study by Tian et al. quantified silver nanoparticle uptake by cyanobacteria using SP-ICP-Q-MS, TOF-ICP-MS, and CyTOF [192]. The study concluded that TOF-ICP-MS is a promising direction for single-cell, single-nanoparticle quantification given its ability to quantify both exogenous nanoparticle elements alongside endogenous cellular elements. SP-ICP-Q-MS performance was poor in comparison due to the single analyte limitations, though it is unclear how the previously discussed dual analyte methods could improve performance in this study. CyTOF performed at a slightly higher level to TOF-ICP-MS in terms of number of detected and paired events but requires the use of additional staining agents to correlate nanoparticle signal with cell signal given the mass cutoff limits of CyTOF filters [192]. The results of this study serve as indicators for the direction of mass spectrometry and elemental analysis research moving forward: TOF-ICP-MS is advantageous given its label-free counting of cells and correlation with nanoparticle events while CyTOF possesses greater accuracy at the cost of requiring cell labeling.

5. Future directions and conclusion

In this review, we detailed current and innovative approaches for high-throughput analysis of single cells that can be applied to transform our understanding of nanoparticle-cell interactions. Flow cytometry approaches allow for the identification of nanoparticle presence and can be used to track differences in nanoparticle uptake or cell association based on shifts in light scattering

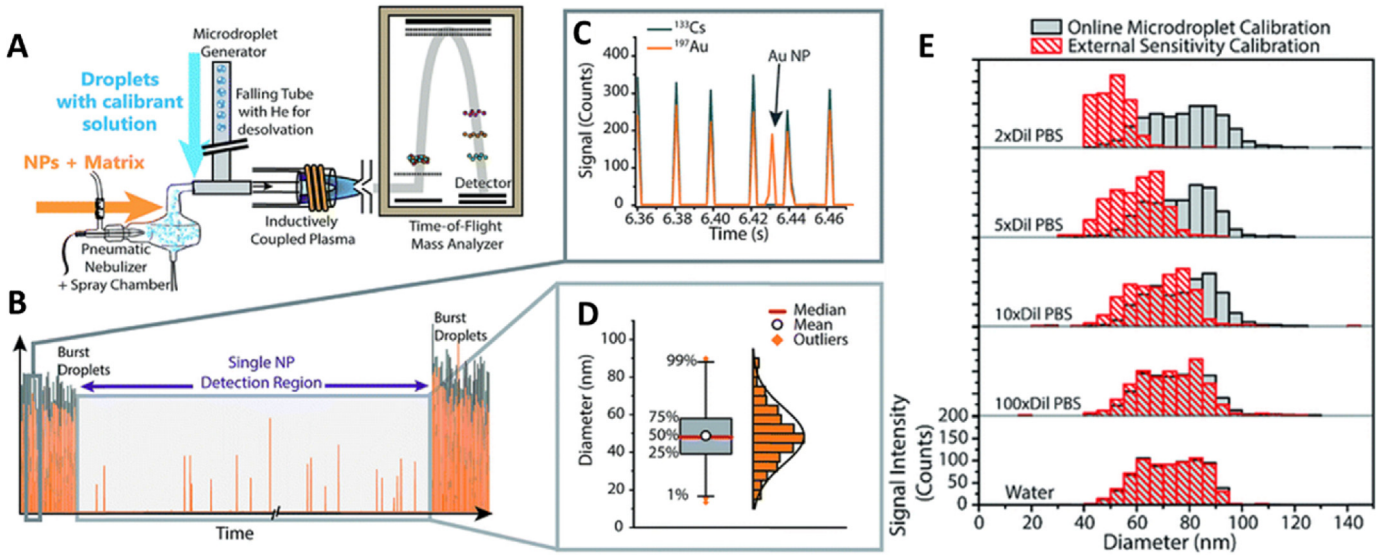

Fig. 7. Online microdroplet methods paired with TOF-ICP-MS overcome sample matrix effects. **(A)** Schematic demonstrating the methodology behind online microdroplet systems. Microdroplets are doped with the ion of interest along with other elements and are added to the sample after nebulization during sample introduction. **(B)** Real-time ionic signal from TOF-ICP-MS measurement of gold nanoparticles with microdroplets. Microdroplets are introduced on the front and back end of sample analysis, allowing for nanoparticle-only identification and quantification in between droplet regimes. **(C)** Gold nanoparticle events are differentiated from microdroplet events as the microdroplets contain multiple overlapping elements. **(D)** After identifying nanoparticle events independent of microdroplets, gold nanoparticle analysis occurs similarly to standard SP-ICP-MS. **(E)** Use of the microdroplet system removes matrix effects from gold nanoparticles suspended in different PBS concentrations, accurately measuring AuNP diameter without suffering from signal attenuation associated with the matrix. Reproduced from Ref. [178] with permission from the Royal Chemistry Society.

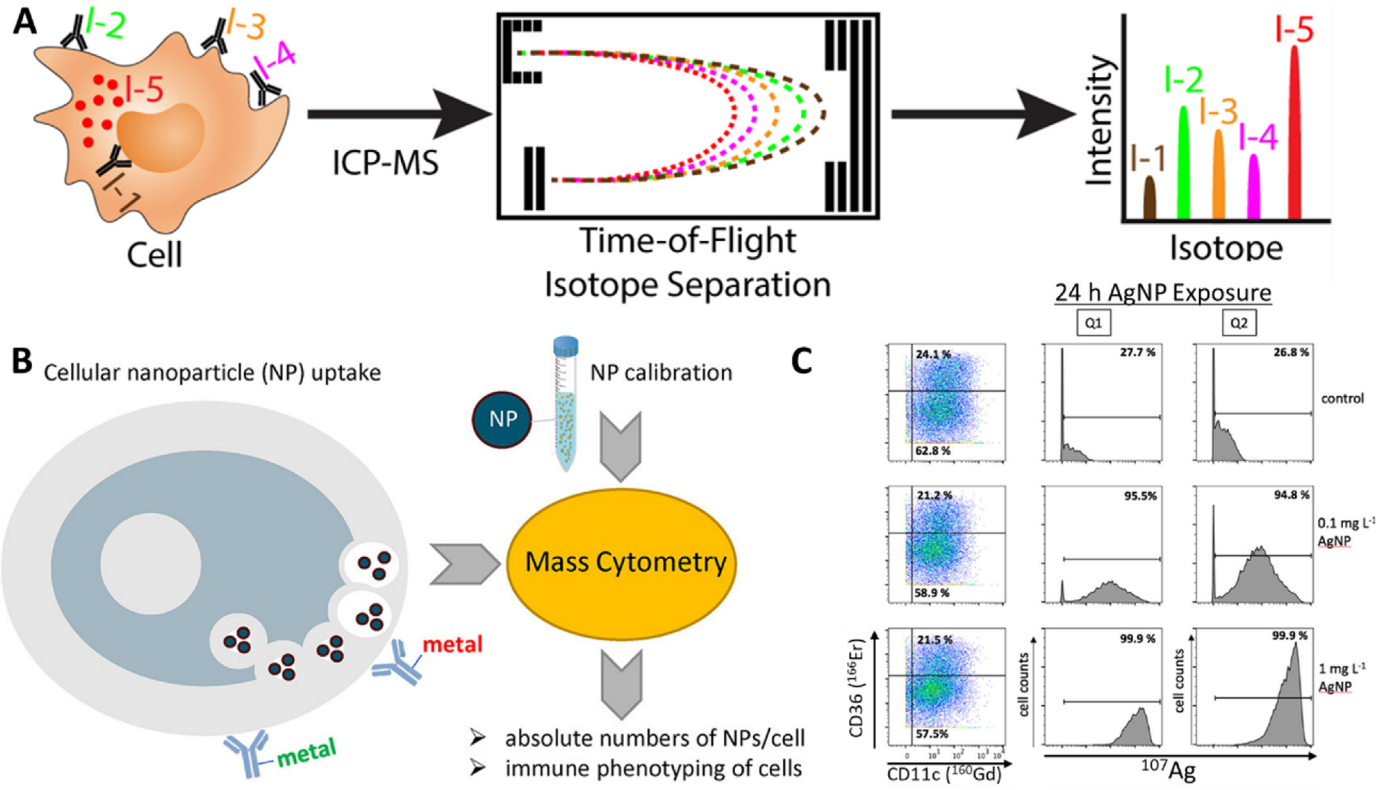

Fig. 8. CyTOF analysis of single cells. **(A)** Schematic of sample introduction and time-of-flight ion separation during CyTOF measurements. Exogenous isotopes can be detected following uptake by cells or labelling with isotope-tagged antibodies. Transient ion signals are separated based on the difference in *m/z* ratio value between isotopes. **(B)** Cells treated with nanoparticles and tagged with metal-bound antibodies can be measured by CyTOF with a nanoparticle calibration solution to quantify nanoparticle uptake of each individual cell. **(C)** Live $CD45^{+}$ cells treated with AgNPs are quantified based on different expression of CD36, with AgNP presence indicated with histograms (middle and right columns). Reprinted with permission from Ref. [181]. Copyright 2023 American Chemical Society.

signals. Despite that, the main limiting factor for conventional flow cytometry is the lack of imaging or imaging resolution that limits the understanding and visualization of cells at the single-level while they pass through the flow chamber. Published studies looked into applying imaging technologies as well as machine learning methods to better answer and understand questions regarding nano-bio cell interactions [47,104,124,125,202]. These methods are exciting avenues for flow cytometry to continue exploring to improve analysis options and workflows. These methods do not only enhance our understanding of nano-bio interactions, as well as the provided visualization of the behavior of the nanoparticles within cells, but they also allow for easier and faster analysis of large sets of data, thus providing increased efficiency.

ICP-MS possesses multiple avenues for single-cell analysis, ranging from relatively affordable SP-ICP-Q-MS methods to more expensive but more informative TOF-ICP-MS. The most limiting factors remain single-analyte restrictions for more conventional single-particle systems (e.g., quadrupole-based mass analyzer systems), complex matrix effects associated with biomedically relevant media and serum samples, and ion cutoff points preventing endogenous element measurement (e.g., phosphorous). Continued investigations into applications of TOF-ICP-MS with microdroplet systems to circumvent matrix effects associated with complex cell suspensions prove to be potentially valuable to the field. Additionally, the ability for TOF-ICP-MS to measure multiple elements simultaneously, including both endogenous cellular elements and exogenous isotopic labels for cell phenotyping, affords expanded opportunity for analysis of nano-bio interactions and nanoparticle distribution in complex cell or tissue samples. Finally, the combination of flow cytometry and mass spectrometry approaches yields mass spectrometry methods that further expand single cell analysis opportunities. The pairing of imaging methods with existing mass cytometry methods seems a rational avenue to continue investing in so as to allow for coinciding visual and spectrometry data to improve quantification of nanoparticle-cell interactions at the single-cell level. Overall, this research has the potential to inform the design of next-generation nanoparticles for safer, more effective, and more efficient applications in nanomedicine.

Funding

This work was supported in part by awards from NIH COBRE (P20GM135009), NSF CAREER (2048130), and OCAST (HR20-106). MH acknowledges funding support via a Dolese Fellowship.

Declaration of competing interest

The authors declare that they have no known competing financial interests or personal relationships that could have appeared to influence the work reported in this paper.

Data availability

Data will be made available on request.

Acknowledgments

The authors thank V. Sheth for fruitful discussions.

References

[1] C. Zhang, L. Yan, X. Wang, S. Zhu, C. Chen, Z. Gu, Y. Zhao, Progress, challenges, and future of nanomedicine, Nano Today 35 (2020). https://doi.org/10.1016/j.nantod.2020.101008.
[2] S. Đorđević, M.M. Gonzalez, I. Conejos-Sánchez, B. Carreira, S. Pozzi, R.C. Acúrcio, R. Satchi-Fainaro, H.F. Florindo, M.J. Vicent, Current hurdles to the translation of nanomedicines from bench to the clinic, Drug Deliv Transl Res 12 (2022) 500–525. https://doi.org/10.1007/s13346-021-01024-2.
[3] S. Mo, P. Tang, W. Luo, L. Zhang, Y. Li, X. Hu, X. Ma, Y. Chen, Y. Bao, X. He, G. Fu, X. Xu, X. Rao, X. Li, R. Guan, S. Chen, Y. Deng, T. Lv, P. Mu, Q. Zheng, S. Wang, F. Liu, Y. Li, W. Sheng, D. Huang, C. Hu, J. Gao, Z. Zhang, S. Cai, H. Clevers, J. Peng, G. Hua, Patient-derived organoids from colorectal cancer with paired liver metastasis reveal tumor heterogeneity and predict response to chemotherapy, Adv. Sci. 9 (2022). https://doi.org/10.1002/advs.202204097.
[4] S. Soares, J. Sousa, A. Pais, C. Vitorino, Nanomedicine: principles, properties, and regulatory issues, Front. Chem. 6 (2018). https://www.frontiersin.org/articles/10.3389/fchem.2018.00360.
[5] M.J. Mitchell, M.M. Billingsley, R.M. Haley, M.E. Wechsler, N.A. Peppas, R. Langer, Engineering precision nanoparticles for drug delivery, Nat. Rev. Drug Discov. 20 (2021) 101–124. https://doi.org/10.1038/s41573-020-0090-8.
[6] N.R.S. Sibuyi, K.L. Moabelo, A.O. Fadaka, S. Meyer, M.O. Onani, A.M. Madiehe, M. Meyer, Multifunctional gold nanoparticles for improved diagnostic and therapeutic applications: a review, Nanoscale Res. Lett. 16 (2021) 174. https://doi.org/10.1186/s11671-021-03632-w.
[7] A.C. Anselmo, S. Mitragotri, Nanoparticles in the clinic, Bioeng Transl Med 1 (2016) 10–29. https://doi.org/10.1002/btm2.10003.
[8] X. Hu, Y. Zhang, T. Ding, J. Liu, H. Zhao, Multifunctional gold nanoparticles: a novel nanomaterial for various medical applications and biological activities, Front. Bioeng. Biotechnol. 8 (2020). https://www.frontiersin.org/articles/10.3389/fbioe.2020.00990.
[9] S. Hua, M.B.C. de Matos, J.M. Metselaar, G. Storm, Current trends and challenges in the clinical translation of nanoparticulate nanomedicines: pathways for translational development and commercialization, Front. Pharmacol. 9 (2018). https://doi.org/10.3389/fphar.2018.00790.
[10] J.J. Rennick, A.P.R. Johnston, R.G. Parton, Key principles and methods for studying the endocytosis of biological and nanoparticle therapeutics, Nat. Nanotechnol. 16 (2021) 266–276. https://doi.org/10.1038/s41565-021-00858-8.
[11] M. Wu, H. Guo, L. Liu, Y. Liu, L. Xie, Size-dependent cellular uptake and localization profiles of silver nanoparticles, Int. J. Nanomed. 14 (2019) 4247–4259.
[12] A.N. Frickenstein, J.M. Hagood, C.N. Britten, B.S. Abbott, M.W. McNally, C.A. Vopat, E.G. Patterson, W.M. MacCuaig, A. Jain, K.B. Walters, L.R. McNally, Mesoporous silica nanoparticles: properties and strategies for enhancing clinical effect, Pharmaceutics 13 (2021). https://doi.org/10.3390/pharmaceutics13040570.
[13] P. Foroozandeh, A.A. Aziz, Insight into cellular uptake and intracellular trafficking of nanoparticles, Nanoscale Res. Lett. 13 (2018) 339. https://doi.org/10.1186/s11671-018-2728-6.
[14] X. Xie, J. Liao, X. Shao, Q. Li, Y. Lin, The effect of shape on cellular uptake of gold nanoparticles in the forms of stars, rods, and triangles, Sci. Rep. 7 (2017) 3827. https://doi.org/10.1038/s41598-017-04229-z.
[15] J. Yue, T.J. Feliciano, W. Li, A. Lee, T.W. Odom, Gold nanoparticle size and shape effects on cellular uptake and intracellular distribution of siRNA nanoconstructs, Bioconjugate Chem. 28 (2017) 1791–1800. https://doi.org/10.1021/acs.bioconjchem.7b00252.
[16] M.P. Vincent, S. Bobbala, N.B. Karabin, M. Frey, Y. Liu, J.O. Navidzadeh, T. Stack, E.A. Scott, Surface chemistry-mediated modulation of adsorbed albumin folding state specifies nanocarrier clearance by distinct macrophage subsets, Nat. Commun. 12 (2021) 648. https://doi.org/10.1038/s41467-020-20886-7.
[17] A. Abdelkhaliq, M. van der Zande, A. Punt, R. Helsdingen, S. Boeren, J.J.M. Vervoort, I.M.C.M. Rietjens, H. Bouwmeester, Impact of nanoparticle surface functionalization on the protein corona and cellular adhesion, uptake and transport, J. Nanobiotechnol. 16 (2018) 70. https://doi.org/10.1186/s12951-018-0394-6.
[18] C.D. Walkey, J.B. Olsen, H. Guo, A. Emili, W.C.W. Chan, Nanoparticle size and surface chemistry determine serum protein adsorption and macrophage uptake, J. Am. Chem. Soc. 134 (2012) 2139–2147. https://doi.org/10.1021/ja2084338.
[19] A. Murschhauser, P.J.F. Röttgermann, D. Woschée, M.F. Ober, Y. Yan, K.A. Dawson, J.O. Rädler, A high-throughput microscopy method for single-cell analysis of event-time correlations in nanoparticle-induced cell death, Commun Biol 2 (2019) 35. https://doi.org/10.1038/s42003-019-0282-0.
[20] M. Steinke, F. Zunhammer, E.I. Chatzopoulou, H. Teller, K. Schütze, H. Walles, J.O. Rädler, C. Grüttner, Rapid analysis of cell–nanoparticle interactions using single-cell Raman trapping microscopy, Angew. Chem. Int. Ed. 57 (2018) 4946–4950. https://doi.org/10.1002/anie.201713151.
[21] F. Wang, S. Wen, H. He, B. Wang, Z. Zhou, O. Shimoni, D. Jin, Microscopic inspection and tracking of single upconversion nanoparticles in living cells, Light Sci. Appl. 7 (2018), 18007. https://doi.org/10.1038/lsa.2018.7.
[22] K.M. McKinnon, Flow cytometry: an overview, Curr. Protoc. Im. (2019) 1–5. https://doi.org/10.1002/cpim.40.
[23] A. Adan, G. Alizada, Y. Kiraz, Y. Baran, A. Nalbant, Flow cytometry: basic principles and applications, Crit. Rev. Biotechnol. 37 (2017) 163–176. https://doi.org/10.3109/07388551.2015.1128876.

[24] S. Wilhelm, R. Bensen, R. Kothapalli, A. Burgett, R. Merrifield, C. Stephan, Quantification of gold nanoparticle uptake into cancer cells using single cell ICP-MS, PerkinElmer Appl Note (2018) 1–4. https://resources.perkinelmer.com/lab-solutions/resources/docs/app_014276_01_nexion_sc-icp-ms_np_uptake_in_cancer_cells.pdf. (Accessed 14 February 2023).
[25] N.D. Donahue, V. Sheth, A.N. Frickenstein, A. Holden, S. Kanapilly, C. Stephan, S. Wilhelm, Absolute quantification of nanoparticle interactions with individual human B cells by single cell mass spectrometry, Nano Lett. 22 (2022) 4192–4199. https://doi.org/10.1021/acs.nanolett.2c01037.
[26] J.M. Njoroge, J.J. Yourick, M.A. Principato, A flow cytometric analysis of macrophage– nanoparticle interactions in vitro: induction of altered Toll-like receptor expression, Int. J. Nanomed. 13 (2018) 8365–8378. https://doi.org/10.2147/IJN.S174184.
[27] R.M. Zucker, K.M. Daniel, E.J. Massaro, S.J. Karafas, L.L. Degn, W.K. Boyes, Detection of silver nanoparticles in cells by flow cytometry using light scatter and far-red fluorescence, Journal of Quantitative Cell Science 83 (2013) 962–972. https://doi.org/10.1002/cyto.22342.
[28] R.M. Zucker, J. Ortenzio, L.L. Degn, J.M. Lerner, W.K. Boyes, Biophysical comparison of four silver nanoparticles coatings using microscopy, hyperspectral imaging and flow cytometry, PLoS One 14 (2019). https://doi.org/10.1371/journal.pone.0219078.
[29] Y. Wu, M.R.K. Ali, K. Dansby, M.A. El-Sayed, Improving the flow cytometry-based detection of the cellular uptake of gold nanoparticles, Anal. Chem. 91 (2019) 14261–14267. https://doi.org/10.1021/acs.analchem.9b02248.
[30] J. Park, M.K. Ha, N. Yang, T.H. Yoon, Flow cytometry-based quantification of cellular Au nanoparticles, Anal. Chem. 89 (2017) 2449–2456. https://doi.org/10.1021/acs.analchem.6b04418.
[31] A. Jochums, E. Friehs, F. Sambale, A. Lavrentieva, D. Bahnemann, T. Scheper, Revelation of different nanoparticle-uptake behavior in two standard cell lines NIH/3T3 and A549 by flow cytometry and time-lapse imaging, Toxics 5 (2017). https://doi.org/10.3390/toxics5030015.
[32] A. Kumar, A.K. Pandey, S.S. Singh, R. Shanker, A. Dhawan, A flow cytometric method to assess nanoparticle uptake in bacteria, Cytometry 79 A (2011) 707–712. https://doi.org/10.1002/cyto.a.21085.
[33] A.R. Arze, N. Manier, A. Chatel, C. Mouneyrac, Characterization of the nano-bio interaction between metallic oxide nanomaterials and freshwater microalgae using flow cytometry, Nanotoxicology 14 (2020) 1082–1095. https://doi.org/10.1080/17435390.2020.1808106ï.
[34] F. Muraca, L. Boselli, V. Castagnola, K.A. Dawson, Ultrasmall gold nanoparticle cellular uptake: influence of transient bionano interactions, ACS Appl. Bio Mater. 3 (2020) 3800–3808. https://doi.org/10.1021/acsabm.0c00379.
[35] X. Wan, M. Liu, M. Ma, D. Chen, N. Wu, L. Li, Z. Li, G. Lin, X. Wang, G. Xu, The ultrasmall biocompatible CuS@BSA nanoparticle and its photothermal effects, Front. Pharmacol. 10 (2019). https://doi.org/10.3389/fphar.2019.00141.
[36] M. Youhannayee, S. Nakhaei-Rad, F. Haghighi, K. Klauke, C. Janiak, M.R. Ahmadian, R. Rabenalt, P. Albers, M. Getzlaff, Physical characterization and uptake of iron oxide nanoparticles of different prostate cancer cells, J. Magn. Magn Mater. 473 (2019) 205–214. https://doi.org/10.1016/J.JMMM.2018.10.062.
[37] B. Chen, Y. Wang, Y. Guo, P. Shi, F. Wang, NaYbF4@NaYF4Nanoparticles: controlled shell growth and shape-dependent cellular uptake, ACS Appl. Mater. Interfaces 13 (2021) 2327–2335. https://doi.org/10.1021/acsami.0c20757.
[38] H. Shin, M. Kwak, T.G. Lee, J.Y. Lee, Quantifying the level of nanoparticle uptake in mammalian cells using flow cytometry, Nanoscale 12 (2020) 15743–15751. https://doi.org/10.1039/d0nr01627f.
[39] H. Garcia Romeu, S. Deville, A. Salvati, Time- and space-resolved flow-cytometry of cell organelles to quantify nanoparticle uptake and intracellular trafficking by cells, Small 17 (2021). https://doi.org/10.1002/smll.202100887.
[40] J. Khetan, M. Shahinuzzaman, S. Barua, D. Barua, Quantitative analysis of the correlation between cell size and cellular uptake of particles, Biophys. J. 116 (2019) 347–359. https://doi.org/10.1016/j.bpj.2018.11.3134.
[41] C.P. Carney, A. Kapur, P. Anastasiadis, R.M. Ritzel, C. Chen, G.F. Woodworth, J.A. Winkles, A.J. Kim, Fn14-Directed DART nanoparticles selectively target neoplastic cells in preclinical models of triple-negative breast cancer brain metastasis, Mol. Pharm. 20 (2023) 314–330. https://doi.org/10.1021/acs.molpharmaceut.2c00663.
[42] Z. Li, T. Li, C. Zhang, J.-S. Ni, Y. Ji, A. Sun, D. Peng, W. Wu, L. Xi, K. Li, A multispectral photoacoustic tracking strategy for wide-field and real-time monitoring of macrophages in inflammation, Anal. Chem. 93 (2021) 8467–8475. https://doi.org/10.1021/acs.analchem.1c00690.
[43] Y. Wang, L. Li, W. Zhao, Y. Dou, H. An, H. Tao, X. Xu, Y. Jia, S. Lu, J. Zhang, H. Hu, Targeted therapy of atherosclerosis by a broad-spectrum reactive oxygen species scavenging nanoparticle with intrinsic anti-inflammatory activity, ACS Nano 12 (2018) 8943–8960. https://doi.org/10.1021/acsnano.8b02037.
[44] E. Puente-Massaguer, P. Saccardo, N. Ferrer-Miralles, M. Lecina, F. Gòdia, Coupling microscopy and flow cytometry for a comprehensive characterization of nanoparticle production in insect cells, Cytometry 97 (2020) 921–932. https://doi.org/10.1002/cyto.a.24033.
[45] S. Vranic, N. Boggetto, V. Contremoulins, S. Mornet, N. Reinhardt, F. Marano, A. Baeza-Squiban, S. Boland, Deciphering the mechanisms of cellular uptake of engineered nanoparticles by accurate evaluation of internalization using imaging flow cytometry, Part. Fibre Toxicol. 10 (2013). https://doi.org/10.1186/1743-8977-10-2.
[46] T. Jin, C. Zhang, F. Liu, X. Chen, G. Liang, F. Ren, S. Liang, C. Song, J. Shi, W. Qiu, X. Jiang, K. Li, L. Xi, On-chip multicolor photoacoustic imaging flow cytometry, Anal. Chem. 93 (2021) 8134–8142. https://doi.org/10.1021/acs.analchem.0c05218.
[47] B.J. Jurgielewicz, Y. Yao, S.L. Stice, Kinetics and specificity of HEK293T extracellular vesicle uptake using imaging flow cytometry, Nanoscale Res. Lett. 15 (2020). https://doi.org/10.1186/s11671-020-03399-6.
[48] A. Görgens, M. Bremer, R. Ferrer-Tur, F. Murke, T. Tertel, P.A. Horn, S. Thalmann, J.A. Welsh, C. Probst, C. Guerin, C.M. Boulanger, J.C. Jones, H. Hanenberg, U. Erdbrügger, J. Lannigan, F.L. Ricklefs, S. El-Andaloussi, B. Giebel, Optimisation of imaging flow cytometry for the analysis of single extracellular vesicles by using fluorescence-tagged vesicles as biological reference material, J. Extracell. Vesicles 8 (2019). https://doi.org/10.1080/20013078.2019.1587567.
[49] J.F. Lusk, C. Miranda, B.S. Smith, Ovarian cancer detection using photoacoustic flow cytometry, JoVE (2019) 2020. https://doi.org/10.3791/60279.
[50] J.F. Lusk, C. Miranda, M. Howell, M. Chrest, J. Eshima, B.S. Smith, Photoacoustic flow system for the detection of ovarian circulating tumor cells utilizing copper sulfide nanoparticles, ACS Biomater. Sci. Eng. 5 (2019) 1553–1560. https://doi.org/10.1021/acsbiomaterials.8b01217.
[51] D.A. Nedosekin, T. Fahmi, Z.A. Nima, J. Nolan, C. Cai, M. Sarimollaoglu, E. Dervishi, A. Basnakian, A.S. Biris, V.P. Zharov, Photoacoustic flow cytometry for nanomaterial research, Photoacoustics 6 (2017) 16–25. https://doi.org/10.1016/J.PACS.2017.03.002.
[52] K. Bhattacharyya, B. Goldschmidt, J. Viator, Detection and capture of breast cancer cells with photoacoustic flow cytometry, J. Biomed. Opt. 21 (2016), 87007. https://doi.org/10.1117/1.jbo.21.8.087007.
[53] A. Sun, T. Li, T. Jin, Y. Li, K. Li, C. Song, L. Xi, Acoustic standing wave aided multiparametric photoacoustic imaging flow cytometry, Anal. Chem. 93 (2021) 14820–14827. https://doi.org/10.1021/acs.analchem.1c03713.
[54] D.A. Nedosekin, J. Nolan, C. Cai, S.E. Bourdo, Z. Nima, A.S. Biris, V.P. Zharov, In vivo noninvasive analysis of graphene nanomaterial pharmacokinetics using photoacoustic flow cytometry, J. Appl. Toxicol. 37 (2017) 1297–1304. https://doi.org/10.1002/jat.3467.
[55] D.A. Nedosekin, M. Khodakovskaya, A.S. Biris, D. Wang, Y. Xu, H. Villagarcia, E.I. Galanzha, V.P. Zharov, In vivo plant flow cytometry: a first proof-of-concept, Cytometry 79 A (2011) 855–865. https://doi.org/10.1002/cyto.a.21128.
[56] E.I. Galanzha, V.P. Zharov, Circulating tumor cell detection and capture by photoacoustic flow cytometry in vivo and ex vivo, Cancers 5 (2013) 1691–1738. https://doi.org/10.3390/cancers5041691.
[57] E.I. Galanzha, E. Shashkov, P.M. Spring, J.Y. Suen, V.P. Zharov, In vivo, noninvasive, label-free detection and eradication of circulating metastatic melanoma cells using two-color photoacoustic flow cytometry with a diode laser, Cancer Res. 69 (2009) 7926–7934. https://doi.org/10.1158/0008-5472.CAN-08-4900.
[58] E.I. Galanzha, E. Shashkov, T. Kelly, J.W. Kim, L. Yang, V.P. Zharov, In vivo magnetic enrichment and multiplex photoacoustic detection of circulating tumour cells, Nat. Nanotechnol. 4 (2009) 855–860. https://doi.org/10.1038/nnano.2009.333.
[59] D. Wei, K. Pang, Q. Song, Y. Suo, H. He, X. Weng, X. Gao, X. Wei, Noninvasive monitoring of nanoparticle clearance and aggregation in blood circulation by in vivo flow cytometry, J. Contr. Release 278 (2018) 66–73. https://doi.org/10.1016/J.JCONREL.2018.03.024.
[60] J. Yao, J. Feng, X. Gao, D. Wei, T. Kang, Q. Zhu, T. Jiang, X. Wei, J. Chen, Neovasculature and circulating tumor cells dual-targeting nanoparticles for the treatment of the highly-invasive breast cancer, Biomaterials 113 (2017) 1–17. https://doi.org/10.1016/J.BIOMATERIALS.2016.10.033.
[61] V.P. Zharov, E.I. Galanzha, E. Shashkov, J.-W. Kim, N.G. Khlebtsov, V. Tuchin, Photoacoustic flow cytometry: principle and application for real-time detection of circulating single nanoparticles, pathogens, and contrast dyes in vivo, J. Biomed. Opt. 12 (2007), 51503. https://doi.org/10.1117/1.2793746.
[62] D.R.A. Stephen, P. Perfetto, Richard Nguyen, Mario Roederer, Richard A. Koup, Kevin L. Holmes, in: Flow Cytometry Protocols, third ed., third ed., Humana Press, 2010. https://doi.org/10.1007/978-1-61737-950-5_1.
[63] G. Maruccio, M.A. Qasaimeh, A. Vembadi, A. Menachery, Cell cytometry: review and perspective on biotechnological advances, cell cytometry: review and perspective on biotechnological advances, Front. Bioeng. Biotechnol. 7 (2019) 147. https://doi.org/10.3389/fbioe.2019.00147.
[64] L. de Rond, E. van der Pol, P.R. Bloemen, T. van den Broeck, L. Monheim, R. Nieuwland, T.G. van Leeuwen, F.A.W. Coumans, A systematic approach to improve scatter sensitivity of a flow cytometer for detection of extracellular vesicles, Cytometry 97 (2020) 582–591. https://doi.org/10.1002/cyto.a.23974.
[65] M. Ghosh, D. Öner, R.C. Duca, S.M. Cokic, S. Seys, S. Kerkhofs, K. van Landuyt, P. Hoet, L. Godderis, Cyto-genotoxic and DNA methylation changes induced by different crystal phases of TiO2-np in bronchial epithelial (16-HBE) cells, Mutat. Res., Fundam. Mol. Mech. Mutagen. 796 (2017) 1–12. https://doi.org/10.1016/J.MRFMMM.2017.01.003.
[66] Y. Ibuki, T. Toyooka, nanoparticle uptake measured by flow cytometry, in: Nanotoxicity, 2012, pp. 157–166. https://doi.org/10.1007/978-1-62703-002-1_11.
[67] L. Taccola, V. Raffa, C. Riggio, O. Vittorio, M.C. Iorio, R. Vanacore, A. Pietrabissa, A. Cuschieri, Zinc oxide nanoparticles as selective killers of proliferating cells, Int. J. Nanomed. 6 (2011) 1129–1140. https://doi.org/

10.2147/IJN.S16581.
[68] R. Chakraborty, D. Leshem-Lev, R. Kornowski, D. Fixler, The scattering of gold nanorods combined with differential uptake, paving a new detection method for macrophage subtypes using flow cytometery, Nano Lett. 20 (2020) 8360–8368. https://doi.org/10.1021/acs.nanolett.0c03525.
[69] J.C. Lee, N.D. Donahue, A.S. Mao, A. Karim, M. Komarneni, E.E. Thomas, E.R. Francek, W. Yang, S. Wilhelm, Exploring maleimide-based nanoparticle surface engineering to control cellular interactions, ACS Appl. Nano Mater. 3 (2020) 2421–2429. https://doi.org/10.1021/acsanm.9b02541.
[70] M.A. Rodrigues, L.A. Beaton-Green, R.C. Wilkins, M.F. Fenech, The potential for complete automated scoring of the cytokinesis block micronucleus cytome assay using imaging flow cytometry, Mutat. Res. Genet. Toxicol. Environ. Mutagen 836 (2018) 53–64. https://doi.org/10.1016/j.mrgentox.2018.05.003.
[71] M.G.H. Pelletier, K. Szymczak, A.M. Barbeau, G.N. Prata, K.S. O'Fallon, P. Gaines, Characterization of neutrophils and macrophages from ex vivo-cultured murine bone marrow for morphologic maturation and functional responses by imaging flow cytometry, Methods 112 (2017) 124–146. https://doi.org/10.1016/j.ymeth.2016.09.005.
[72] J. Lannigan, U. Erdbruegger, Imaging flow cytometry for the characterization of extracellular vesicles, Methods 112 (2017) 55–67. https://doi.org/10.1016/j.ymeth.2016.09.018.
[73] S.M. Manohar, P. Shah, A. Nair, Flow cytometry: principles, applications and recent advances, Bioanalysis 13 (2021) 185–202. https://doi.org/10.4155/bio-2020-0267.
[74] K.T. Soh, P.K. Wallace, RNA flow cytometry using the branched DNA technique, in: Methods in Molecular Biology, Humana Press Inc., 2018, pp. 49–77. https://doi.org/10.1007/978-1-4939-7346-0_4.
[75] X. Li, B. Fan, L. Liu, D. Chen, S. Cao, D. Men, J. Wang, J. Chen, A microfluidic fluorescent flow cytometry capable of quantifying cell sizes and numbers of specific cytosolic proteins, Sci. Rep. 8 (2018). https://doi.org/10.1038/s41598-018-32333-1.
[76] L. Ferrer-Font, C. Pellefigues, J.U. Mayer, S.J. Small, M.C. Jaimes, K.M. Price, Panel design and optimization for high-dimensional immunophenotyping assays using spectral flow cytometry, Curr Protoc Cytom 92 (2020). https://doi.org/10.1002/cpcy.70.
[77] L. Ferrer-Font, P. Mehta, P. Harmos, A.J. Schmidt, S. Chappell, K.M. Price, I.F. Hermans, F. Ronchese, G. le Gros, J.U. Mayer, High-dimensional analysis of intestinal immune cells during helminth infection, Elife 9 (2020). https://doi.org/10.7554/eLife.51678.
[78] S.M. Manohar, P. Shah, A. Nair, Flow cytometry: principles, applications and recent advances, Bioanalysis 13 (2021) 185–202. https://doi.org/10.4155/bio-2020-0267.
[79] A. Rossi, I. Pacella, S. Piconese, RNA flow cytometry for the study of T cell metabolism, Int. J. Mol. Sci. 22 (2021). https://doi.org/10.3390/ijms22083906.
[80] A.P. Frei, F.A. Bava, E.R. Zunder, E.W.Y. Hsieh, S.Y. Chen, G.P. Nolan, P.F. Gherardini, Highly multiplexed simultaneous detection of RNAs and proteins in single cells, Nat. Methods 13 (2016) 269–275. https://doi.org/10.1038/nmeth.3742.
[81] K.T. Soh, P.K. Wallace, RNA flow cytometry using the branched DNA technique, in: Methods in Molecular Biology, Humana Press Inc., 2018, pp. 49–77. https://doi.org/10.1007/978-1-4939-7346-0_4.
[82] M.B. Hanley, W. Lomas, D. Mittar, V. Maino, E. Park, Detection of low abundance RNA molecules in individual cells by flow cytometry, PLoS One 8 (2013). https://doi.org/10.1371/journal.pone.0057002.
[83] D.L. Bonilla, G. Reinin, E. Chua, Full spectrum flow cytometry as a powerful technology for cancer immunotherapy research, Front. Mol. Biosci. 7 (2021). https://doi.org/10.3389/fmolb.2020.612801.
[84] L. Li, S. Wang, J. Xue, Y. Lin, L. Su, C. Xue, C. Mao, N. Cai, Y. Tian, S. Zhu, L. Wu, X. Yan, Development of spectral nano-flow cytometry for high-throughput multiparameter analysis of individual biological nanoparticles, Anal. Chem. (2022). https://doi.org/10.1021/acs.analchem.2c05159.
[85] L.M. Park, J. Lannigan, M.C. Jaimes, OMIP-069: forty-color full spectrum flow cytometry panel for deep immunophenotyping of major cell subsets in human peripheral blood, Cytometry 97 (2020) 1044–1051. https://doi.org/10.1002/cyto.a.24213.
[86] J.P. Nolan, The evolution of spectral flow cytometry, Cytometry 101 (2022) 812–817. https://doi.org/10.1002/cyto.a.24566.
[87] Y. Tian, C. Xue, W. Zhang, C. Chen, L. Ma, Q. Niu, L. Wu, X. Yan, Refractive index determination of individual viruses and small extracellular vesicles in aqueous media using nano-flow cytometry, Anal. Chem. 94 (2022) 14299–14307. https://doi.org/10.1021/acs.analchem.2c02833.
[88] K. Gao, H. Lian, C. Xue, J. Zhou, X. Yan, High-throughput counting and sizing of therapeutic protein aggregates in the nanometer size range by nano-flow cytometry, Anal. Chem. 94 (2022) 17634–17644. https://doi.org/10.1021/acs.analchem.2c04382.
[89] H. Liu, Y. Tian, C. Xue, Q. Niu, C. Chen, X. Yan, Analysis of extracellular vesicle DNA at the single-vesicle level by nano-flow cytometry, J. Extracell. Vesicles 11 (2022). https://doi.org/10.1002/jev2.12206.
[90] Q. Niu, L. Ma, S. Zhu, L. Li, Q. Zheng, J. Hou, H. Lian, L. Wu, X. Yan, Quantitative assessment of the physical virus titer and purity by ultrasensitive flow virometry, Angew. Chem. Int. Ed. 60 (2021) 9351–9356. https://doi.org/10.1002/anie.202100872.
[91] H. Lian, S. He, C. Chen, X. Yan, Flow cytometric analysis of nanoscale biological particles and organelles, Annu. Rev. Anal. Chem. 12 (2019) 389–409. https://doi.org/10.1146/annurev-anchem-061318-115042.
[92] K.M. Danielson, J. Estanislau, J. Tigges, V. Toxavidis, V. Camacho, E.J. Felton, J. Khoory, S. Kreimer, A.R. Ivanov, P.Y. Mantel, J. Jones, P. Akuthota, S. Das, I. Ghiran, Diurnal variations of circulating extracellular vesicles measured by nano flow cytometry, PLoS One 11 (2016). https://doi.org/10.1371/journal.pone.0144678.
[93] J.P. Nolan, D. Condello, Spectral flow cytometry, Curr Protoc Cytom (2013). https://doi.org/10.1002/0471142956.cy0127s63.
[94] Y. Tian, M. Gong, Y. Hu, H. Liu, W. Zhang, M. Zhang, X. Hu, D. Aubert, S. Zhu, L. Wu, X. Yan, Quality and efficiency assessment of six extracellular vesicle isolation methods by nano-flow cytometry, J. Extracell. Vesicles 9 (2020). https://doi.org/10.1080/20013078.2019.1697028.
[95] D. Choi, L. Montermini, H. Jeong, S. Sharma, B. Meehan, J. Rak, Mapping subpopulations of cancer cell-derived extracellular vesicles and particles by nano-flow cytometry, ACS Nano 13 (2019) 10499–10511. https://doi.org/10.1021/acsnano.9b04480.
[96] G. Holzner, B. Mateescu, D. van Leeuwen, G. Cereghetti, R. Dechant, S. Stavrakis, A. deMello, High-throughput multiparametric imaging flow cytometry: toward diffraction-limited sub-cellular detection and monitoring of sub-cellular processes, Cell Rep. 34 (2021), 108824. https://doi.org/10.1016/J.CELREP.2021.108824.
[97] D.A. Basiji, W.E. Ortyn, L. Liang, V. Venkatachalam, P. Morrissey, Cellular image analysis and imaging by flow cytometry, Clinics in Laboratory Medicing 27 (2007) 653–670. https://doi.org/10.1016/j.cll.2007.05.008.
[98] G. Wu, Y. Zhao, X. Li, M.M. Ali, S. Jia, Y. Ren, L. Hu, Single-cell extracellular vesicle analysis by microfluidics and beyond, TrAC, Trends Anal. Chem. 159 (2023), 116930. https://doi.org/10.1016/J.TRAC.2023.116930.
[99] D.M.D. Siu, K.C.M. Lee, M.C.K. Lo, S. Stassen, M. Wang, I.Z.Q. Zhang, H.K.H. So, G.C.F. Chan, K.S.E. Cheah, K.K.Y. Wong, M.K.Y. Hsin, J.C.M. Ho, K.K. Tsia, Deep-learning-assisted biophysical imaging cytometry at massive throughput delineates cell population heterogeneity, Lab Chip 20 (2020) 3696–3708. https://doi.org/10.1039/d0lc00542h.
[100] S. Stavrakis, G. Holzner, J. Choo, A. deMello, High-throughput microfluidic imaging flow cytometry, Curr. Opin. Biotechnol. 55 (2019) 36–43. https://doi.org/10.1016/j.copbio.2018.08.002.
[101] Y. Han, Y. Gu, A.C. Zhang, Y.H. Lo, Review: imaging technologies for flow cytometry, Lab Chip 16 (2016) 4639–4647. https://doi.org/10.1039/c6lc01063f.
[102] P. Rees, H.D. Summers, A. Filby, A.E. Carpenter, M. Doan, Imaging flow cytometry, Nature Reviews Methods Primers 2 (2022). https://doi.org/10.1038/s43586-022-00167-x.
[103] T.K. Kaiser, M. Khorenko, A. Moussavi, M. Engelke, S. Boretius, C. Feldmann, H.M. Reichardt, Highly selective organ distribution and cellular uptake of inorganic-organic hybrid nanoparticles customized for the targeted delivery of glucocorticoids, J. Contr. Release 319 (2020) 360–370. https://doi.org/10.1016/J.JCONREL.2020.01.010.
[104] M. Lippeveld, C. Knill, E. Ladlow, A. Fuller, L.J. Michaelis, Y. Saeys, A. Filby, D. Peralta, Classification of human white blood cells using machine learning for stain-free imaging flow cytometry, Cytometry 97 (2020) 308–319. https://doi.org/10.1002/cyto.a.23920.
[105] T. Blasi, H. Hennig, H.D. Summers, F.J. Theis, J. Cerveira, J.O. Patterson, D. Davies, A. Filby, A.E. Carpenter, P. Rees, Label-free cell cycle analysis for high-throughput imaging flow cytometry, Nat. Commun. 7 (2016). https://doi.org/10.1038/ncomms10256.
[106] J. Botha, H.R. Pugsley, A. Handberg, Conventional, high-resolution and imaging flow cytometry: benchmarking performance in characterisation of extracellular vesicles, Biomedicines 9 (2021) 1–24. https://doi.org/10.3390/biomedicines9020124.
[107] L. Wu, W.W. Woud, C.C. Baan, D.A. Hesselink, E. van der Pol, G. Jenster, K. Boer, Isolation-free measurement of single urinary extracellular vesicles by imaging flow cytometry, Nanomedicine 48 (2023), 102638. https://doi.org/10.1016/J.NANO.2022.102638.
[108] W.W. Woud, E. van der Pol, E. Mul, M.J. Hoogduijn, C.C. Baan, K. Boer, A. Merino, An imaging flow cytometry-based methodology for the analysis of single extracellular vesicles in unprocessed human plasma, Commun Biol 5 (2022). https://doi.org/10.1038/s42003-022-03569-5.
[109] F.L. Ricklefs, C.L. Maire, R. Reimer, L. Dührsen, K. Kolbe, M. Holz, E. Schneider, A. Rissiek, A. Babayan, C. Hille, K. Pantel, S. Krasemann, M. Glatzel, D.H. Heiland, J. Flitsch, T. Martens, N.O. Schmidt, S. Peine, X.O. Breakefield, S. Lawler, E.A. Chiocca, B. Fehse, B. Giebel, A. Görgens, M. Westphal, K. Lamszus, Imaging flow cytometry facilitates multiparametric characterization of extracellular vesicles in malignant brain tumours, J. Extracell. Vesicles 8 (2019). https://doi.org/10.1080/20013078.2019.1588555.
[110] T. Tertel, A. Görgens, B. Giebel, Analysis of individual extracellular vesicles by imaging flow cytometry, Methods Enzymol. 645 (2020) 55–78. https://doi.org/10.1016/BS.MIE.2020.05.013.
[111] Y. Ofir-Birin, P. Abou karam, A. Rudik, T. Giladi, Z. Porat, N. Regev-Rudzki, Monitoring extracellular vesicle cargo active uptake by imaging flow cytometry, Front. Immunol. 9 (2018). https://doi.org/10.3389/fimmu.2018.01011.
[112] K. O'Brien, K. Breyne, S. Ughetto, L.C. Laurent, X.O. Breakefield, RNA delivery by extracellular vesicles in mammalian cells and its applications, Nat. Rev. Mol. Cell Biol. 21 (2020) 585–606. https://doi.org/10.1038/s41580-020-0251-y.

[113] L. Czernek, M. Düchler, Functions of cancer-derived extracellular vesicles in immunosuppression, Arch. Immunol. Ther. Exp. 65 (2017) 311–323. https://doi.org/10.1007/s00005-016-0453-3.
[114] M. Malloci, L. Perdomo, M. Veerasamy, R. Andriantsitohaina, G. Simard, M. Carmen Martínez, H. Antelmann, M. Bachschmid, D. Becker, G. Semenza, C.K. sen Malloci, Extracellular vesicles: mechanisms in human health and disease, Antioxidants and Redux Signaling 30 (2019). https://doi.org/10.1089/ars.2017.7265.
[115] M. Takasugi, Emerging roles of extracellular vesicles in cellular senescence and aging, Aging Cell 17 (2018). https://doi.org/10.1111/acel.12734.
[116] S. Mastoridis, G.M. Bertolino, G. Whitehouse, F. Dazzi, A. Sanchez-Fueyo, M. Martinez-Llordella, Multiparametric analysis of circulating exosomes and other small extracellular vesicles by advanced imaging flow cytometry, Front. Immunol. 9 (2018). https://doi.org/10.3389/fimmu.2018.01583.
[117] B.J. Jurgielewicz, Y. Yao, S.L. Stice, Kinetics and specificity of HEK293T extracellular vesicle uptake using imaging flow cytometry, Nanoscale Res. Lett. 15 (2020). https://doi.org/10.1186/s11671-020-03399-6.
[118] N. Nitta, T. Sugimura, A. Isozaki, H. Mikami, K. Hiraki, S. Sakuma, T. Iino, F. Arai, T. Endo, Y. Fujiwaki, H. Fukuzawa, M. Hase, T. Hayakawa, K. Hiramatsu, Y. Hoshino, M. Inaba, T. Ito, H. Karakawa, Y. Kasai, K. Koizumi, S.W. Lee, C. Lei, M. Li, T. Maeno, S. Matsusaka, D. Murakami, A. Nakagawa, Y. Oguchi, M. Oikawa, T. Ota, K. Shiba, H. Shintaku, Y. Shirasaki, K. Suga, Y. Suzuki, N. Suzuki, Y. Tanaka, H. Tezuka, C. Toyokawa, Y. Yalikun, M. Yamada, M. Yamagishi, T. Yamano, A. Yasumoto, Y. Yatomi, M. Yazawa, D. di Carlo, Y. Hosokawa, S. Uemura, Y. Ozeki, K. Goda, Intelligent image-activated cell sorting, Cell 175 (2018) 266–276. https://doi.org/10.1016/j.cell.2018.08.028. e13.
[119] Y. Gu, A.C. Zhang, Y. Han, J. Li, C. Chen, Y.H. Lo, Machine learning based real-time image-guided cell sorting and classification, Cytometry 95 (2019) 499–509. https://doi.org/10.1002/cyto.a.23764.
[120] D. Schraivogel, T.M. Kuhn, B. Rauscher, M. Rodríguez-Martínez, M. Paulsen, K. Owsley, A. Middlebrook, C. Tischer, B. Ramasz, D. Ordoñez-Rueda, M. Dees, S. Cuylen-Haering, E. Diebold, L.M. Steinmetz, High-speed fluorescence image-enabled cell sorting, Science 375 (2022) 315–320. https://doi.org/10.1126/science.abj3013.
[121] A. Kleiber, D. Kraus, T. Henkel, W. Fritzsche, Review: tomographic imaging flow cytometry, Lab Chip 21 (2021) 3655–3666. https://doi.org/10.1039/d1lc00533b.
[122] F. Merola, P. Memmolo, L. Miccio, R. Savoia, M. Mugnano, A. Fontana, G. D'Ippolito, A. Sardo, A. Iolascon, A. Gambale, P. Ferraro, Tomographic flow cytometry by digital holography, Light Sci. Appl. 6 (2017). https://doi.org/10.1038/lsa.2016.241.
[123] A. Kleiber, D. Kraus, T. Henkel, W. Fritzsche, Review: tomographic imaging flow cytometry, Lab Chip 21 (2021) 3655–3666. https://doi.org/10.1039/D1LC00533B.
[124] M. Doan, I. Vorobjev, P. Rees, A. Filby, O. Wolkenhauer, A.E. Goldfeld, J. Lieberman, N. Barteneva, A.E. Carpenter, H. Hennig, Diagnostic potential of imaging flow cytometry, Trends Biotechnol. 36 (2018) 649–652. https://doi.org/10.1016/j.tibtech.2017.12.008.
[125] M. Nassar, M. Doan, A. Filby, O. Wolkenhauer, D.K. Fogg, J. Piasecka, C.A. Thornton, A.E. Carpenter, H.D. Summers, P. Rees, H. Hennig, Label-free identification of white blood cells using machine learning, Cytometry 95 (2019) 836–842. https://doi.org/10.1002/cyto.a.23794.
[126] P. Rees, J.W. Wills, M.R. Brown, J. Tonkin, M.D. Holton, N. Hondow, A.P. Brown, R. Brydson, V. Millar, A.E. Carpenter, H.D. Summers, Nanoparticle vesicle encoding for imaging and tracking cell populations, Nat. Methods 11 (2014) 1177–1181. https://doi.org/10.1038/nmeth.3105.
[127] H. Mikami, M. Kawaguchi, C.J. Huang, H. Matsumura, T. Sugimura, K. Huang, C. Lei, S. Ueno, T. Miura, T. Ito, K. Nagasawa, T. Maeno, H. Watarai, M. Yamagishi, S. Uemura, S. Ohnuki, Y. Ohya, H. Kurokawa, S. Matsusaka, C.W. Sun, Y. Ozeki, K. Goda, Virtual-freezing fluorescence imaging flow cytometry, Nat. Commun. 11 (2020). https://doi.org/10.1038/s41467-020-14929-2.
[128] M. Sarimollaoglu, D.A. Nedosekin, Y.A. Menyaev, M.A. Juratli, V.P. Zharov, Nonlinear photoacoustic signal amplification from single targets in absorption background, Photoacoustics 2 (2014) 1–11. https://doi.org/10.1016/J.PACS.2013.11.002.
[129] R.H. Edgar, A.-P. Samson, T. Kocsis, J.A. Viator, Photoacoustic flow cytometry using functionalized microspheres for selective detection of bacteria, Micromachines 14 (2023). https://doi.org/10.3390/mi14030573.
[130] R.H. Edgar, J. Cook, C. Noel, A. Minard, A. Sajewski, M. Fitzpatrick, R. Fernandez, J.D. Hempel, J.A. Kellum, J.A. Viator, Bacteriophage-mediated identification of bacteria using photoacoustic flow cytometry, J. Biomed. Opt. 24 (2019), 115003. https://doi.org/10.1117/1.JBO.24.11.115003.
[131] F. Liu, T. Jin, R. Yan, T. Li, B. Hu, L. Yao, T. Huang, C. Song, L. Xi, An opto-acousto-fluidic microscopic system with a high spatiotemporal resolution for microfluidic applications, Opt Express 27 (2019) 1425. https://doi.org/10.1364/oe.27.001425.
[132] E.I. Galanzha, V.P. Zharov, Photoacoustic flow cytometry, Methods 57 (2012) 280–296. https://doi.org/10.1016/j.ymeth.2012.06.009.
[133] Y. Suo, Z. Gu, X. Wei, Advances of in vivo flow cytometry on cancer studies, Cytometry 97 (2020) 15–23. https://doi.org/10.1002/cyto.a.23851.
[134] C. Cai, K.A. Carey, D.A. Nedosekin, Y.A. Menyaev, M. Sarimollaoglu, E.I. Galanzha, J.S. Stumhofer, V.P. Zharov, In vivo photoacoustic flow cytometry for early malaria diagnosis, Cytometry 89 (2016) 531–542. https://doi.org/10.1002/cyto.a.22854.
[135] V.v. Tuchin, A. Tárnok, V.P. Zharov, In vivo flow cytometry: a horizon of opportunities, Cytometry 79 A (2011) 737–745. https://doi.org/10.1002/cyto.a.21143.
[136] X. Tan, R. Patil, P. Bartosik, J.M. Runnels, C.P. Lin, M. Niedre, In vivo flow cytometry of extremely rare circulating cells, Sci. Rep. 9 (2019). https://doi.org/10.1038/s41598-019-40143-2.
[137] S. Wilschefski, M. Baxter, Inductively coupled plasma mass spectrometry: introduction to analytical aspects, Clin. Biochem. Rev. 40 (2019) 115–133. https://doi.org/10.33176/AACB-19-00024.
[138] R. Chemnitzer, Strategies for achieving the lowest possible detection limits in ICP-MS, Spectroscopy 34 (2019) 12–16.
[139] A.N. Frickenstein, S. Mukherjee, T. Harcourt, Y. He, V. Sheth, L. Wang, Z. Malik, S. Wilhelm, Quantification of monodisperse and biocompatible gold nanoparticles by single-particle ICP-MS, Anal. Bioanal. Chem. (2023). https://doi.org/10.1007/s00216-023-04540-x.
[140] W. Yang, L. Wang, M. Fang, V. Sheth, Y. Zhang, A.M. Holden, N.D. Donahue, D.E. Green, A.N. Frickenstein, E.M. Mettenbrink, T.A. Schwemley, E.R. Francek, M. Haddad, M.N. Hossen, S. Mukherjee, S. Wu, P.L. DeAngelis, S. Wilhelm, Nanoparticle surface engineering with heparosan polysaccharide reduces serum protein adsorption and enhances cellular uptake, Nano Lett. 22 (2022) 2103–2111. https://doi.org/10.1021/acs.nanolett.2c00349.
[141] W. Yang, A.N. Frickenstein, V. Sheth, A. Holden, E.M. Mettenbrink, L. Wang, A.A. Woodward, B.S. Joo, S.K. Butterfield, N.D. Donahue, D.E. Green, A.G. Thomas, T. Harcourt, H. Young, M. Tang, Z.A. Malik, R.G. Harrison, P. Mukherjee, P.L. DeAngelis, S. Wilhelm, Controlling nanoparticle uptake in innate immune cells with heparosan polysaccharides, Nano Lett. 22 (2022) 7119–7128. https://doi.org/10.1021/acs.nanolett.2c02226.
[142] Y. Zhang, C.K. Elechalawar, W. Yang, A.N. Frickenstein, S. Asfa, K.-M. Fung, B.N. Murphy, S.K. Dwivedi, G. Rao, A. Dey, S. Wilhelm, R. Bhattacharya, P. Mukherjee, Disabling partners in crime: gold nanoparticles disrupt multicellular communications within the tumor microenvironment to inhibit ovarian tumor aggressiveness, Mater. Today 56 (2022) 79–95. https://doi.org/10.1016/j.mattod.2022.01.025.
[143] J. Noireaux, R. Grall, M. Hullo, S. Chevillard, C. Oster, E. Brun, C. Sicard-Roselli, K. Loeschner, P. Fisicaro, Gold nanoparticle uptake in tumor cells: quantification and size distribution by sp-ICPMS, Separations 6 (2019). https://doi.org/10.3390/separations6010003.
[144] R.C. Merrifield, C. Stephan, J.R. Lead, Quantification of Au nanoparticle biouptake and distribution to freshwater algae using single cell – ICP-MS, Environ. Sci. Technol. 52 (2018) 2271–2277. https://doi.org/10.1021/acs.est.7b04968.
[145] A. López-Serrano Oliver, S. Baumgart, W. Bremser, S. Flemig, D. Wittke, A. Grützkau, A. Luch, A. Haase, N. Jakubowski, Quantification of silver nanoparticles taken up by single cells using inductively coupled plasma mass spectrometry in the single cell measurement mode, J Anal At Spectrom 33 (2018) 1256–1263. https://doi.org/10.1039/C7JA00395A.
[146] I. Zanoni, M. Crosera, E. Pavoni, G. Adami, M. Mauro, A.L. Costa, J.R. Lead, F. Larese Filon, Use of single particle ICP-MS to estimate silver nanoparticle penetration through baby porcine mucosa, Nanotoxicology 15 (2021) 1005–1015. https://doi.org/10.1080/17435390.2021.1940338.
[147] J.T.-S. Lum, K.S.-Y. Leung, Quantifying silver nanoparticle association and elemental content in single cells using dual mass mode in quadrupole-based inductively coupled plasma-mass spectrometry, Anal. Chim. Acta 1061 (2019) 50–59. https://doi.org/10.1016/j.aca.2019.02.042.
[148] J. Jiménez-Lamana, J. Wojcieszek, M. Jakubiak, M. Asztemborska, J. Szpunar, Single particle ICP-MS characterization of platinum nanoparticles uptake and bioaccumulation by Lepidium sativum and Sinapis alba plants, J Anal At Spectrom 31 (2016) 2321–2329. https://doi.org/10.1039/C6JA00201C.
[149] L. Amable, C. Stephan, S. Smith, R. Merrifield, An Introduction to Single Cell ICP-MS Analysis, PerkinElmer Appl Note, 2017. https://resources.perkinelmer.com/lab-solutions/resources/docs/wht-introduction-to-single-cell-icp-ms-012774a_01.pdf. (Accessed 14 February 2023).
[150] Z. Chen, B. Chen, M. He, B. Hu, Negative magnetophoresis focusing microchips online-coupled with ICP–MS for high-throughput single-cell analysis, Anal. Chem. 94 (2022) 6649–6656. https://doi.org/10.1021/acs.analchem.1c04216.
[151] Y. Jiao, L. Gao, Y. Ji, W. Liu, Recent advances in microfluidic single-cell analysis and its applications in drug development, TrAC, Trends Anal. Chem. 157 (2022), 116796. https://doi.org/10.1016/j.trac.2022.116796.
[152] X. Zhang, X. Wei, X. Men, Z. Jiang, W.-Q. Ye, M.-L. Chen, T. Yang, Z.-R. Xu, J.-H. Wang, Inertial-force-Assisted, high-throughput, droplet-free, single-cell sampling coupled with ICP-MS for real-time cell analysis, Anal. Chem. 92 (2020) 6604–6612. https://doi.org/10.1021/acs.analchem.0c00376.
[153] M. Corte-Rodríguez, R. Álvarez-Fernández, P. García-Cancela, M. Montes-Bayón, J. Bettmer, Single cell ICP-MS using on line sample introduction systems: current developments and remaining challenges, TrAC, Trends Anal. Chem. 132 (2020), 116042. https://doi.org/10.1016/j.trac.2020.116042.
[154] K.-H. Chun, J.T.-S. Lum, K.S.-Y. Leung, Dual-elemental analysis of single particles using quadrupole-based inductively coupled plasma-mass spectrometry, Anal. Chim. Acta 1192 (2022), 339389. https://doi.org/10.1016/j.aca.2021.339389.
[155] N.D. Donahue, S. Kanapilly, C. Stephan, M.C. Marlin, E.R. Francek, M. Haddad, J. Guthridge, S. Wilhelm, Quantifying chemical composition and reaction kinetics of individual colloidally dispersed nanoparticles, Nano Lett. 22

(2022) 294–301. https://doi.org/10.1021/acs.nanolett.1c03752.
[156] K. Ding, S. Liang, C. Xie, Q. Wan, C. Jin, S. Wang, Y.-T. Tang, M. Zhang, R. Qiu, Discrimination and quantification of soil nanoparticles by dual-analyte single particle ICP–QMS, Anal. Chem. 94 (2022) 10745–10753. https://doi.org/10.1021/acs.analchem.2c01379.
[157] P.A. Doble, R.G. de Vega, D.P. Bishop, D.J. Hare, D. Clases, Laser ablation–inductively coupled plasma–mass spectrometry imaging in biology, Chem. Rev. 121 (2021) 11769–11822. https://doi.org/10.1021/acs.chemrev.0c01219.
[158] S. Theiner, A. Schweikert, C. Haberler, A. Peyrl, G. Koellensperger, Laser ablation-ICP-TOFMS imaging of germ cell tumors of patients undergoing platinum-based chemotherapy, Metallomics 12 (2020) 1246–1252. https://doi.org/10.1039/d0mt00080a.
[159] A. Sussulini, J.S. Becker, J.S. Becker, Laser ablation ICP-MS: application in biomedical research, Mass Spectrom. Rev. 36 (2017) 47–57. https://doi.org/10.1002/mas.21481.
[160] T. van Acker, S.J.M. van Malderen, M. van Heerden, J.E. McDuffie, F. Cuyckens, F. Vanhaecke, High-resolution laser ablation-inductively coupled plasma-mass spectrometry imaging of cisplatin-induced nephrotoxic side effects, Anal. Chim. Acta 945 (2016) 23–30. https://doi.org/10.1016/j.aca.2016.10.014.
[161] A. Schoeberl, M. Gutmann, S. Theiner, M. Schaier, A. Schweikert, W. Berger, G. Koellensperger, Cisplatin uptake in macrophage subtypes at the single-cell level by LA-ICP-TOFMS imaging, Anal. Chem. 93 (2021) 16456–16465. https://doi.org/10.1021/acs.analchem.1c03442.
[162] C.J. Greenhalgh, E. Karekla, G.J. Miles, I.R. Powley, C. Costa, J. de Jesus, M.J. Bailey, C. Pritchard, M. MacFarlane, J.H. Pringle, A.J. Managh, Exploration of matrix effects in laser ablation inductively coupled plasma mass spectrometry imaging of cisplatin-treated tumors, Anal. Chem. 92 (2020) 9847–9855. https://doi.org/10.1021/acs.analchem.0c01347.
[163] M. Wang, L. Zheng, B. Wang, P. Yang, H. Fang, S. Liang, W. Chen, W. Feng, Laser ablation-single particle-inductively coupled plasma mass spectrometry as a sensitive tool for bioimaging of silver nanoparticles in vivo degradation, Chin. Chem. Lett. 33 (2022) 3484–3487. https://doi.org/10.1016/j.cclet.2022.03.098.
[164] S.G. Elci, B. Yan, S.T. Kim, K. Saha, Y. Jiang, G.A. Klemmer, D.F. Moyano, G.Y. Tonga, V.M. Rotello, R.W. Vachet, Quantitative imaging of 2 nm monolayer-protected gold nanoparticle distributions in tissues using laser ablation inductively-coupled plasma mass spectrometry (LA-ICP-MS), Analyst 141 (2016) 2418–2425. https://doi.org/10.1039/C6AN00123H.
[165] I.-L. Hsiao, F.S. Bierkandt, P. Reichardt, A. Luch, Y.-J. Huang, N. Jakubowski, J. Tentschert, A. Haase, Quantification and visualization of cellular uptake of TiO2 and Ag nanoparticles: comparison of different ICP-MS techniques, J. Nanobiotechnol. 14 (2016) 50. https://doi.org/10.1186/s12951-016-0203-z.
[166] L.-N. Zheng, L.-X. Feng, J.-W. Shi, H.-Q. Chen, B. Wang, M. Wang, H.-F. Wang, W.-Y. Feng, Single-cell isotope dilution analysis with LA–ICP–MS: a new approach for quantification of nanoparticles in single cells, Anal. Chem. 92 (2020) 14339–14345. https://doi.org/10.1021/acs.analchem.0c01775.
[167] L.-N. Zheng, Y.-B. Sang, R.-P. Luo, B. Wang, F.-T. Yi, M. Wang, W.-Y. Feng, Determination of silver nanoparticles in single cells by microwell trapping and laser ablation ICP-MS determination, J Anal At Spectrom 34 (2019) 915–921. https://doi.org/10.1039/C8JA00438B.
[168] K. Löhr, O. Borovinskaya, G. Tourniaire, U. Panne, N. Jakubowski, Arraying of single cells for quantitative high throughput laser ablation ICP-TOF-MS, Anal. Chem. 91 (2019) 11520–11528. https://doi.org/10.1021/acs.analchem.9b00198.
[169] L. Hendriks, A. Gundlach-Graham, B. Hattendorf, D. Günther, Characterization of a new ICP-TOFMS instrument with continuous and discrete introduction of solutions, J Anal At Spectrom 32 (2017) 548–561. https://doi.org/10.1039/C6JA00400H.
[170] S. Harycki, A. Gundlach-Graham, Characterization of a high-sensitivity ICP-TOFMS instrument for microdroplet, nanoparticle, and microplastic analyses, J Anal At Spectrom 38 (2023) 111–120. https://doi.org/10.1039/D2JA00295G.
[171] D.E. Salt, I. Baxter, B. Lahner, Ionomics and the study of the plant ionome, Annu. Rev. Plant Biol. 59 (2008) 709–733. https://doi.org/10.1146/annurev.arplant.59.032607.092942.
[172] M. Malinouski, N.M. Hasan, Y. Zhang, J. Seravalli, J. Lin, A. Avanesov, S. Lutsenko, V.N. Gladyshev, Genome-wide RNAi ionomics screen reveals new genes and regulation of human trace element metabolism, Nat. Commun. 5 (2014) 3301. https://doi.org/10.1038/ncomms4301.
[173] M. von der Au, O. Borovinskaya, L. Flamigni, K. Kuhlmeier, C. Büchel, B. Meermann, Single cell-inductively coupled plasma-time of flight-mass spectrometry approach for ecotoxicological testing, Algal Res. 49 (2020), 101964. https://doi.org/10.1016/j.algal.2020.101964.
[174] M.I. Chronakis, M. von der Au, B. Meermann, Single cell-asymmetrical flow field-flow fractionation/ICP-time of flight-mass spectrometry (sc-AF4/ICP-ToF-MS): an efficient alternative for the cleaning and multielemental analysis of individual cells, J Anal At Spectrom 37 (2022) 2691–2700. https://doi.org/10.1039/D2JA00264G.
[175] L. Hendriks, L. Michael Skjolding, Thomas Robert, Single-cell analysis by inductively coupled plasma–time-of-flight mass spectrometry to quantify algal cell interaction with nanoparticles by their elemental fingerprint, Spectroscopy 35 (2020) 9–16.
[176] T.-S. Lum, K. Sze-Yin Leung, Strategies to overcome spectral interference in ICP-MS detection, J Anal At Spectrom 31 (2016) 1078–1088. https://doi.org/10.1039/C5JA00497G.
[177] S.H. Tan, G. Horlick, Matrix-effect observations in inductively coupled plasma mass spectrometry, J Anal At Spectrom 2 (1987) 745–763. https://doi.org/10.1039/JA9870200745.
[178] L. Hendriks, B. Ramkorun-Schmidt, A. Gundlach-Graham, J. Koch, R.N. Grass, N. Jakubowski, D. Günther, Single-particle ICP-MS with online microdroplet calibration: toward matrix independent nanoparticle sizing, J Anal At Spectrom 34 (2019) 716–728. https://doi.org/10.1039/C8JA00397A.
[179] K. Mehrabi, D. Günther, A. Gundlach-Graham, Single-particle ICP-TOFMS with online microdroplet calibration for the simultaneous quantification of diverse nanoparticles in complex matrices, Environ Sci Nano 6 (2019) 3349–3358. https://doi.org/10.1039/C9EN00620F.
[180] S. Harycki, A. Gundlach-Graham, Online microdroplet calibration for accurate nanoparticle quantification in organic matrices, Anal. Bioanal. Chem. 414 (2022) 7543–7551. https://doi.org/10.1007/s00216-022-04115-2.
[181] A. López-Serrano Oliver, A. Haase, A. Peddinghaus, D. Wittke, N. Jakubowski, A. Luch, A. Grützkau, S. Baumgart, Mass cytometry enabling absolute and fast quantification of silver nanoparticle uptake at the single cell level, Anal. Chem. 91 (2019) 11514–11519. https://doi.org/10.1021/acs.analchem.9b01870.
[182] A. Ivask, A.J. Mitchell, C.M. Hope, S.C. Barry, E. Lombi, N.H. Voelcker, Single cell level quantification of nanoparticle–cell interactions using mass cytometry, Anal. Chem. 89 (2017) 8228–8232. https://doi.org/10.1021/acs.analchem.7b01006.
[183] A. Malysheva, A. Ivask, C.L. Doolette, N.H. Voelcker, E. Lombi, Cellular binding, uptake and biotransformation of silver nanoparticles in human T lymphocytes, Nat. Nanotechnol. 16 (2021) 926–932. https://doi.org/10.1038/s41565-021-00914-3.
[184] Y.S.S. Yang, P.U. Atukorale, K.D. Moynihan, A. Bekdemir, K. Rakhra, L. Tang, F. Stellacci, D.J. Irvine, High-throughput quantitation of inorganic nanoparticle biodistribution at the single-cell level using mass cytometry, Nat. Commun. 8 (2017). https://doi.org/10.1038/ncomms14069.
[185] M.H. Spitzer, G.P. Nolan, Mass cytometry: single cells, many features, Cell 165 (2016) 780–791. https://doi.org/10.1016/j.cell.2016.04.019.
[186] L.P. Arnett, R. Rana, W.W.-Y. Chung, X. Li, M. Abtahi, D. Majonis, J. Bassan, M. Nitz, M.A. Winnik, Reagents for mass cytometry, Chem Rev (2023). https://doi.org/10.1021/acs.chemrev.2c00350.
[187] H. Drescher, S. Weiskirchen, R. Weiskirchen, Flow cytometry: a blessing and a curse, Biomedicines 9 (2021). https://doi.org/10.3390/biomedicines9111613.
[188] S.D. Tanner, V.I. Baranov, O.I. Ornatsky, D.R. Bandura, T.C. George, An introduction to mass cytometry: fundamentals and applications, Cancer Immunology, Immunotherapy 62 (2013) 955–965. https://doi.org/10.1007/s00262-013-1416-8.
[189] S.C. Bendall, E.F. Simonds, P. Qiu, E.A.D. Amir, P.O. Krutzik, R. Finck, R.v. Bruggner, R. Melamed, A. Trejo, O.I. Ornatsky, R.S. Balderas, S.K. Plevritis, K. Sachs, D. Pe'er, S.D. Tanner, G.P. Nolan, Single-cell mass cytometry of differential immune and drug responses across a human hematopoietic continuum, Science 332 (2011) 687–696. https://doi.org/10.1126/science.1198704.
[190] B. Sahaf, A. Rahman, H.T. Maecker, S.C. Bendall, High-parameter immune profiling with CyTOF, in: M. Thurin, A. Cesano, F.M. Marincola (Editors), Biomarkers for Immunotherapy of Cancer: Methods and Protocols, Springer New York, New York, NY, 2020, pp. 351–368. https://doi.org/10.1007/978-1-4939-9773-2_16.
[191] R. Gadalla, B. Noamani, B.L. MacLeod, R.J. Dickson, M. Guo, W. Xu, S. Lukhele, H.J. Elsaesser, A.R.A. Razak, N. Hirano, T.L. McGaha, B. Wang, M. Butler, C.J. Guidos, P.S. Ohashi, L.L. Siu, D.G. Brooks, Validation of CyTOF against flow cytometry for immunological studies and monitoring of human cancer clinical trials, Front. Oncol. 9 (2019). https://doi.org/10.3389/fonc.2019.00415.
[192] X. Tian, H. Jiang, M. Wang, W. Cui, Y. Guo, L. Zheng, L. Hu, G. Qu, Y. Yin, Y. Cai, G. Jiang, Exploring the performance of quadrupole, time-of-flight, and multi-collector ICP-MS for dual-isotope detection on single nanoparticles and cells, Anal. Chim. Acta 1240 (2023), 340756. https://doi.org/10.1016/j.aca.2022.340756.
[193] A.F. Nassar, H. Ogura, A. Wisnewski, Impact of recent innovations in the use of mass cytometry in support of drug development, Drug Discov. Today 20 (2015) 1169–1175. https://doi.org/10.1016/j.drudis.2015.06.001.
[194] D.R. Bandura, V.I. Baranov, O.I. Ornatsky, A. Antonov, R. Kinach, X. Lou, S. Pavlov, S. Vorobiev, J.E. Dick, S.D. Tanner, Mass cytometry: technique for real time single cell multitarget immunoassay based on inductively coupled plasma time-of-flight mass spectrometry, Anal. Chem. 81 (2009) 6813–6822. https://doi.org/10.1021/ac901049w.
[195] Y.P. Zhu, T. Eggert, D.J. Araujo, P. Vijayanand, C.H. Ottensmeier, C.C. Hedrick, CyTOF mass cytometry reveals phenotypically distinct human blood neutrophil populations differentially correlated with melanoma stage, J Immunother Cancer 8 (2020), e000473. https://doi.org/10.1136/jitc-2019-000473.
[196] M.K. Ha, S.J. Kwon, J.-S. Choi, N.T. Nguyen, J. Song, Y. Lee, Y.-E. Kim, I. Shin, J.-W. Nam, T.H. Yoon, Mass cytometry and single-cell RNA-seq profiling of the heterogeneity in human peripheral blood mononuclear cells interacting with silver nanoparticles, Small 16 (2020), 1907674. https://doi.org/10.1002/

smll.201907674.
[197] A.R. Schulz, S. Stanislawiak, S. Baumgart, A. Grützkau, H.E. Mei, Silver nanoparticles for the detection of cell surface antigens in mass cytometry, Cytometry 91 (2017) 25–33. https://doi.org/10.1002/cyto.a.22904.
[198] J. Pichaandi, L. Tong, A. Bouzekri, Q. Yu, O. Ornatsky, V. Baranov, M.A. Winnik, Liposome-encapsulated NaLnF4 nanoparticles for mass cytometry: evaluating nonspecific binding to cells, Chem. Mater. 29 (2017) 4980–4990. https://doi.org/10.1021/acs.chemmater.7b01339.
[199] Q. Chang, O.I. Ornatsky, I. Siddiqui, A. Loboda, V.I. Baranov, D.W. Hedley, Imaging Mass Cytometry, Cytometry Part A 91 (2017) 160–169. https://doi.org/10.1002/cyto.a.23053.
[200] H.R. Ali, H.W. Jackson, V.R.T. Zanotelli, E. Danenberg, J.R. Fischer, H. Bardwell, E. Provenzano, O.M. Rueda, S.F. Chin, S. Aparicio, C. Caldas, B. Bodenmiller, Imaging mass cytometry and multiplatform genomics define the phenogenomic landscape of breast cancer, Nat. Can. (Que.) 1 (2020) 163–175. https://doi.org/10.1038/s43018-020-0026-6.
[201] B. Malile, J. Brkic, A. Bouzekri, D.J. Wilson, O. Ornatsky, C. Peng, J.I.L. Chen, DNA-conjugated gold nanoparticles as high-mass probes in imaging mass cytometry, ACS Appl. Bio Mater. 2 (2019) 4316–4323. https://doi.org/10.1021/acsabm.9b00574.
[202] Y. Gu, A.C. Zhang, Y. Han, J. Li, C. Chen, Y.H. Lo, Machine learning based real-time image-guided cell sorting and classification, Cytometry 95 (2019) 499–509. https://doi.org/10.1002/cyto.a.23764.